Reactive scalar field near the turbulent/non-turbulent interface in a planar jet with a second-order chemical reaction

Cite as: Phys. Fluids **26**, 105111 (2014); https://doi.org/10.1063/1.4900403
Submitted: 14 April 2014 • Accepted: 13 October 2014 • Published Online: 30 October 2014

T. Watanabe, Y. Sakai, K. Nagata, et al.

PHYSICS OF FLUIDS **26**, 105111 (2014)

Reactive scalar field near the turbulent/non-turbulent interface in a planar jet with a second-order chemical reaction

T. Watanabe,[1,a)] Y. Sakai,[1] K. Nagata,[1] Y. Ito,[1] and T. Hayase[2]
[1]*Department of Mechanical Science and Engineering, Nagoya University, Nagoya, Japan*
[2]*Institute of Fluid Science, Tohoku University, Sendai, Japan*

(Received 14 April 2014; accepted 13 October 2014; published online 30 October 2014)

The reactive scalar field near the turbulent/non-turbulent (T/NT) interface is analyzed using a direct numerical simulation (DNS) of a planar jet with an isothermal second-order chemical reaction A + B → P. Reactants A and B are supplied from the jet and ambient flows, respectively. The DNS of the reactive jet is performed for Damköhler numbers $Da = 0.1$, 1, and 10. A visualization of the T/NT interface shows that most of the product P is contained in the turbulent region. The conditional mean concentrations of the reactive species change sharply near the T/NT interface. The width of the jump in the conditional mean concentration is almost independent of the chemical species and the Damköhler number. For the slow reaction ($Da = 0.1$), the conditional average of the chemical production rate gradually increases from the non-turbulent region toward the turbulent region. In contrast, the conditional average of the production rate for $Da = 1$ and 10 has a large peak value slightly inside the T/NT interface. The chemical reaction near the T/NT interface strongly depends on the interface orientation. The reactant A is deficient near the T/NT interface. The production rate is large near the interface toward which the deficient reactant A is frequently transported by the velocity fields. The transport due to the velocity relative to the interface movement strongly depends on the relationship between the interface geometry and the mean flow field. The dependence of the chemical reaction on the interface orientation becomes strong as Da increases. When the interface propagates toward the non-turbulent region, the reactant A and product P are contained in the turbulent region although the molecular diffusion and reaction contribute to the increase in the concentrations of A (non-reactive case) and P in the non-turbulent region. In contrast, the interface propagation toward the turbulent region leaves the fluids containing A and P in the non-turbulent region.
[http://dx.doi.org/10.1063/1.4900403]

I. INTRODUCTION

Chemical reactions are often observed in turbulent flows in the environment or in industrial equipment. The process of chemical reactions is important for designing chemical reactors and predicting pollutant transformation in the environment. In non-premixed systems, chemical reactions occur when the reactants mix.[1] When two reactants are separated into two flows, they become mixed and the chemical reaction occurs initially in the interfacial region of the two flows.[2–4] This region is often called the reaction zone and appears near a surface of stoichiometric mixture.[5] Therefore, mixing near the reaction zone significantly affects the chemical reaction, and the characteristics of the reaction zone are often used for modeling turbulent reactive flows (e.g., the flamelet model[6]).

An interface that divides turbulent and non-turbulent flows can be seen in free shear flows, such as wakes, jets, and mixing layers. The turbulent/non-turbulent (T/NT) interface plays an important role

[a)]Research Fellow of the Japan Society for the Promotion of Science. Electronic mail: watanabe.tomoaki@c.nagoya-u.jp

in the development of free shear flows. When reactants are separately supplied to a free shear flow, mixing of the reactants and chemical reactions start near the T/NT interface. The chemical products diffuse with the development of the flow, which arises from the spreading of the turbulent region. Therefore, the mixing and chemical reactions near the T/NT interface are expected to determine the characteristics of the reactive scalar fields in free shear flows. As shown by Gampert *et al.*,[7] a stoichiometric mixture fraction appears near the T/NT interface in various types of jet flames. Thus, the characteristics of chemical reactions near the T/NT interface are also important for modeling the chemical reactions in free shear flows.

The turbulent region is characterized by high vorticity, and the T/NT interface can be detected by thresholding the vorticity magnitude. Therefore, direct numerical simulations (DNSs) are useful for investigating the T/NT interface because they provide all the components of the vorticity vector. Bisset *et al.* used a DNS to investigate the characteristics of the flow and scalar fields near the T/NT interface in wakes behind a flat plate.[8] They introduced the conditional statistics conditioned on the distance from the T/NT interface. DNSs of temporally developing jets were performed by da Silva *et al.*[9] to analyze the invariants of the velocity gradient, rate of strain, and rate of rotation tensors,[10] thickness of the T/NT interface,[11] vorticity structure near the T/NT interface,[12] kinetic energy budget,[13] and viscous superlayer.[14]

When vorticity data are not available, a passive scalar is often used as a marker of the turbulent region instead of the vorticity vector. Westerweel *et al.* detected the T/NT interface in a round jet using a diffusive dye.[15–17] They simultaneously measured the velocity and concentration in the round jet using particle image velocimetry and laser-induced fluorescence to experimentally investigate the velocity and scalar fields near the T/NT interface. They showed that the entrainment process is dominated by small-scale eddies near the T/NT interface.[16] Holzner *et al.* experimentally investigated the turbulent front generated by an oscillating grid using particle tracking velocimetry and analyzed the acceleration of fluid particles, enstrophy, and rate of strain near the T/NT interface.[18,19] They showed that the viscous process dominates the propagation of the T/NT interface.[20] However, large-scale motions of non-turbulent fluids are also responsible for the total entrainment process.[21]

Previous studies on the T/NT interface have investigated the characteristics of the flow and non-reactive scalar fields near the interface. However, data on the reactive scalar field near the T/NT interface are lacking. In this work, we investigate a reactive scalar field near the T/NT interface in a planar jet with an isothermal chemical reaction $A + B \rightarrow P$. The time average, average in the turbulent region, and conditional average conditioned on the distance from the T/NT interface are analyzed. Watanabe *et al.* showed that the enstrophy transport mechanism significantly depends on the interface orientation using a DNS of a spatially developing jet.[22–25] We investigate the dependence of the chemical reaction near the T/NT interface on the interface orientation. Then, we show that the chemical reaction near the T/NT interface is affected by the interface characteristics. The transport of the concentration near the T/NT interface is also analyzed to elucidate the mechanism by which concentrations of the reactive species diffuse. Section II describes the DNS of the reactive planar jet. In Sec. III, the reactive scalar field near the T/NT interface is analyzed. Finally, the conclusion is summarized in Sec. IV.

II. DIRECT NUMERICAL SIMULATION OF A REACTIVE PLANAR JET

The DNS results for a reactive planar jet[22] are used to investigate the reactive scalar field near the T/NT interface. We consider the passive scalar transport in an incompressible planar jet with an isothermal one-step irreversible chemical reaction $A + B \rightarrow P$. Figure 1 shows a sketch of the flow field and coordinate system. The jet flow containing the reactant A is injected into the ambient flow containing the reactant B through a slit with a width of d. The product P is produced by the chemical reaction. For simplicity, all the species are assumed to have equal molecular diffusivities D. The origin of the coordinate system is located at the center of the jet inlet. The streamwise, cross-streamwise, and spanwise directions are represented by x, y, and z, respectively. The mixture

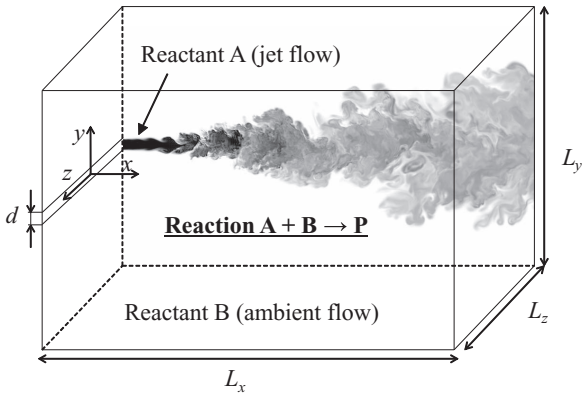

FIG. 1. Planar jet with isothermal chemical reaction.

fraction ξ can be defined as

$$\xi = \frac{\Gamma_A - \Gamma_B + \Gamma_{B0}}{\Gamma_{A0} + \Gamma_{B0}}. \tag{1}$$

The mixture fraction is the non-reactive scalar whose value is zero in the ambient flow and one at the jet inlet. Here, Γ_α is the instantaneous concentration of species α, and $\Gamma_{\alpha 0}$ is the initial concentration of species α. The governing equations of the flow field are the continuity equation and Navier–Stokes equations:

$$\frac{\partial U_j}{\partial x_j} = 0, \tag{2}$$

$$\frac{\partial U_i}{\partial t} + \frac{\partial U_j U_i}{\partial x_j} = -\frac{\partial p}{\partial x_i} + \nu \frac{\partial^2 U_i}{\partial x_j \partial x_j}. \tag{3}$$

Here, U_i is the instantaneous velocity component, p is the instantaneous pressure divided by the density ρ, and ν is the kinematic viscosity. The governing equations for the reactive scalar field are the transport equations for the mixture fraction and concentration of the product P, which are written as follows:

$$\frac{\partial \xi}{\partial t} + \frac{\partial U_j \xi}{\partial x_j} = D \frac{\partial^2 \xi}{\partial x_j \partial x_j}, \tag{4}$$

$$\frac{\partial \Gamma_P}{\partial t} + \frac{\partial U_j \Gamma_P}{\partial x_j} = D \frac{\partial^2 \Gamma_P}{\partial x_j \partial x_j} + S_P. \tag{5}$$

Here, S_α is the chemical source term for reactive species α, which is given by

$$S_P = -S_A = -S_B = k \Gamma_A \Gamma_B. \tag{6}$$

Here, k is the reaction rate constant. The concentrations of the reactants A and B can be calculated using the mass conservation law:

$$\Gamma_A = \Gamma_{A0} \xi - \Gamma_P, \tag{7}$$

$$\Gamma_B = \Gamma_{B0}(1 - \xi) - \Gamma_P. \tag{8}$$

The governing equations are solved using a finite difference method. The fully conservative fourth-order central difference scheme[26] is used for spatial discretization in the x and z directions, and the fully conservative second-order central difference scheme[26] is used in the y direction. The continuity equation and Navier–Stokes equations are solved using the fractional step method. The Poisson equation is solved by the conjugate gradient method. The Crank–Nicolson method is used for the

TABLE I. Coefficients in Eqs. (9) and (10) used to determine the boundary condition at the jet inlet.

n	0	1	2	3	4	5
A_n	1.303×10^{0}	-9.236×10^{-1}	-8.571×10^{0}	-1.207×10^{2}	3.464×10^{2}	0
$B_{u,n}$	4.673×10^{-2}	5.470×10^{-2}	-1.368×10^{0}	1.043×10^{1}	-1.657×10^{1}	0
$B_{v,n}$	3.505×10^{-2}	-1.558×10^{-2}	5.192×10^{-1}	-1.249×10^{0}	0	0
$B_{w,n}$	3.505×10^{-2}	-3.551×10^{-3}	1.930×10^{-1}	-1.186×10^{0}	7.355×10^{0}	-1.267×10^{1}

time integration of the y direction viscous and molecular diffusion terms, whereas the third-order Runge–Kutta method is used for the other terms. This hybrid implicit/explicit scheme was proposed and used in Spalart *et al.*[27] The size of the computational domain is $L_x \times L_y \times L_z = 13.5\pi d \times 11.0\,\pi d \times 2.6\pi d$, and $N_x \times N_y \times N_z = 700 \times 430 \times 74$ computational grid points are used. The grid is equidistant in the x and z directions. In the y direction, a fine grid is used near the jet centerline. The Reynolds number based on the width of the jet inlet (d) and the mean bulk velocity at the jet inlet (U_J) is $Re = U_J d/\nu = 2200$, and the Schmidt number $Sc = \nu/D$ is 1. The Damköhler number, which is the ratio of the time scale of a flow to that of a chemical reaction, is defined as $Da = k(\Gamma_{A0} + \Gamma_{B0})d/U_J$. The DNS is performed for $Da = 0.1$, 1, and 10 by adjusting the reaction rate constant k. According to experimental studies of a liquid jet with a chemical reaction,[28–31] the initial concentration ratio of the reactants A and B is set to $\Gamma_{A0}/\Gamma_{B0} = 2$. The stoichiometric value of the mixture fraction is $\xi_S = \Gamma_{B0}/(\Gamma_{A0} + \Gamma_{B0}) = 0.333$. The maximum concentration of the product P in the stoichiometric mixture is $\Gamma_{P0} = \Gamma_{A0}\Gamma_{B0}/(\Gamma_{A0} + \Gamma_{B0})$. The mean streamwise velocity of the ambient flow at $x = 0$ is $U_A = 0.056U_J$.

We use the measurement results[28–31] for the mean velocity and rms value of the streamwise velocity fluctuation at the jet inlet to determine the boundary condition. Random fluctuations are superimposed on the mean velocity profile to generate the inflow velocity at the jet inlet so that the cross-streamwise profiles of the streamwise mean velocity (U_{in}) and the rms values of the velocity fluctuations (u_{rms}, v_{rms}, w_{rms}) satisfy the following equations at the jet inlet:

$$\frac{U_{in}(y) - U_A}{U_J} = \sum_{n=0}^{5} A_n \left(\frac{y}{d}\right)^{2n}, \tag{9}$$

$$\frac{u_{rms}(y)}{U_J} = \sum_{n=0}^{5} B_{u,n} \left|\frac{y}{d}\right|^{n}, \quad \frac{v_{rms}(y)}{U_J} = \sum_{n=0}^{5} B_{v,n} \left|\frac{y}{d}\right|^{n}, \quad \frac{w_{rms}(y)}{U_J} = \sum_{n=0}^{5} B_{w,n} \left|\frac{y}{d}\right|^{n}. \tag{10}$$

The coefficients, A_n, $B_{u,n}$, $B_{v,n}$, and $B_{w,n}$, are summarized in Table I. Figure 2 shows the measurement results[28–31] for $U_{in}(y)$ and $u_{rms}(y)$ and the values from Eqs. (9) and (10). In the ambient flow at

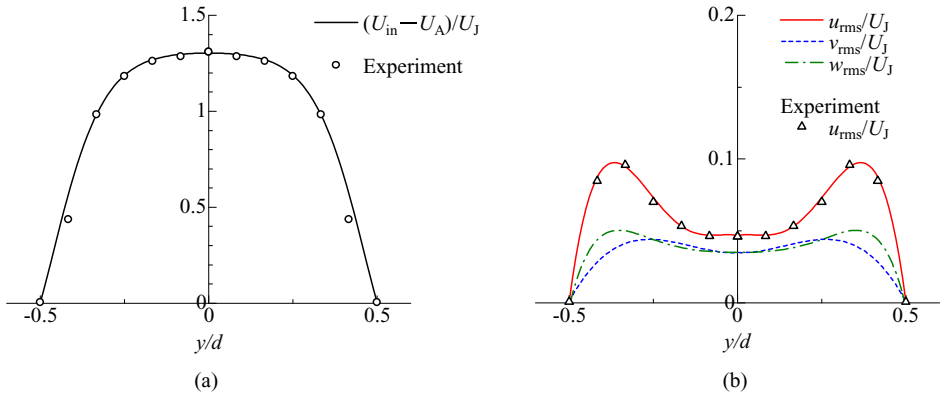

FIG. 2. (a) Mean streamwise velocity and (b) rms values of velocity fluctuations at jet inlet. Cross-streamwise profiles of velocity statistics at jet inlet are compared with measurement results.[28–31]

$x = 0$, the streamwise velocity is set to U_A without any fluctuations. At $x = 0$, the y and z direction components of the mean velocity are set to zero. At $y = 0$ at the jet inlet, the integral length scale is $0.051d$ and the turbulent Reynolds number is $Re_\lambda = u_{rms}\lambda_x/\nu = 3.0$. Here, the integral length scale is obtained from the integral time scale by using the Taylor hypothesis of a frozen turbulence, $\lambda_i = \sqrt{\langle u_i^2\rangle/\langle(\partial u_i/\partial x_i)^2\rangle}$ is the Taylor microscale, $u_i = U_i - \langle U_i\rangle$ is the fluctuating component of the i direction velocity, and $\langle\ \rangle$ denotes a time-averaged value, which is calculated by taking the time-average and average in the spanwise (z) direction in the DNS. As in a DNS of the planar jet,[32] Re_λ increases near the jet inlet with the jet development. In the present DNS, the values of Re_λ are 77.1 and 79.8 at $x/d = 10$ and 30 on the jet centerline, respectively. The convective boundary condition[33] is applied to the y–z plane at $x = L_x$. At the lateral boundaries, the y-directional gradient of velocity is set to zero, and the periodic boundary condition is applied to the spanwise direction. At the lateral boundaries and y-z plane at $x = 0$, the concentrations of the reactive species are imposed to satisfy $\Gamma_A = \Gamma_{A0}$ and $\Gamma_B = \Gamma_P = 0$ at the jet inlet, and $\Gamma_B = \Gamma_{B0}$ and $\Gamma_A = \Gamma_P = 0$ in the ambient flow.

At the initial time step, the velocity in the computational domain is set to the mean velocity in the ambient flow at $x = 0$ ($U = U_A$, $V = W = 0$), and the mixture fraction and concentration of P are set to zero. The conditional statistics explained below are calculated after a time $t = 2400d/U_J$. We confirmed that the flow and scalar fields reached a statistically stationary state before $t = 1200d/U_J$.

III. RESULTS AND DISCUSSION

A. Time-averaged characteristics of the reactive jet

The time-averaged characteristics of the velocity and mixture fraction are compared with the experimental results[28–31] to validate the DNS results. In the experiment,[28–31] Sc for the mixture fraction was about 600. However, the difference in Sc has small influence on the mean mixture fraction profile when Sc is not too small because the molecular diffusion term is negligible in the averaged scalar transport equation.[34] Figure 3 shows the mean characteristics of streamwise velocity and mixture fraction. Here, U_C and ξ_C denote the mean streamwise velocity and mean mixture fraction on the jet centerline, respectively. The jet half-widths based on $\langle U\rangle - U_A$ and $\langle\xi\rangle$ are denoted by b_U and b_ξ, respectively. The results show that the streamwise development of $\langle U\rangle$ and $\langle\xi\rangle$ agrees well with the experimental results. $U_C - U_A$ and ξ_C decrease in proportion to $(x/d)^{-1/2}$, and b_U and b_ξ increase in proportion to (x/d). The self-similar profiles appear in the cross-streamwise profiles of $\langle U\rangle$ and $\langle\xi\rangle$. Thus, the typical characteristics of the self-similar planar jet are observed in the present DNS results. The mean flow development strongly depends on the inflow velocity.[35] The agreement in the mean fields between the DNS and the experiment justifies the inflow velocity generation method.

Figures 4 and 5 show the cross-streamwise profiles of $\langle\Gamma_A\rangle$ and $\langle\Gamma_P\rangle$, respectively. $\langle\Gamma_A\rangle$ is decreased by the chemical reaction. In the downstream direction, the difference in $\langle\Gamma_A\rangle$ between the reactive and non-reactive cases becomes large and $\langle\Gamma_P\rangle$ increases because the chemical reaction progresses. At $x/d = 38$, most of the reactant A is consumed for $Da = 10$ in the outer region. $\langle\Gamma_P\rangle$ has a peak value away from the jet centerline at $x/d = 10$ and 15 but is large near the jet centerline at $x/d = 38$. For the mean concentrations of reactive species, the self-similarity does not exist because the chemical consumption and production significantly change the cross-streamwise profiles of the mean concentrations.

The chemical production rate of P normalized by U_J, d, and Γ_{P0} is given by $\hat{S}_P = Da\hat{\Gamma}_A\hat{\Gamma}_B$, where $\hat{\Gamma}_\alpha = \Gamma_\alpha/\Gamma_{\alpha0}$ is the normalized concentration. Figure 6 shows the cross-streamwise profiles of $\langle\hat{S}_P\rangle$. $\langle\hat{S}_P\rangle$ has a peak value at $y/b_\xi \approx 0.85$ for $Da = 10$ at $x/d = 10$ and 15, but is almost independent of the cross-streamwise location for $Da = 0.1$ near the jet centerline at $x/d = 10$. Because of small concentration of A for $Da = 1$ and 10 at $x/d = 38$ [Fig. 4(c)], the mean production rate at these Da values is small in this region.

In the planar jet, the cross-streamwise component is important in turbulent diffusion of a mean scalar.[34] Therefore, we investigate the cross-streamwise turbulent mass flux of reactive species.

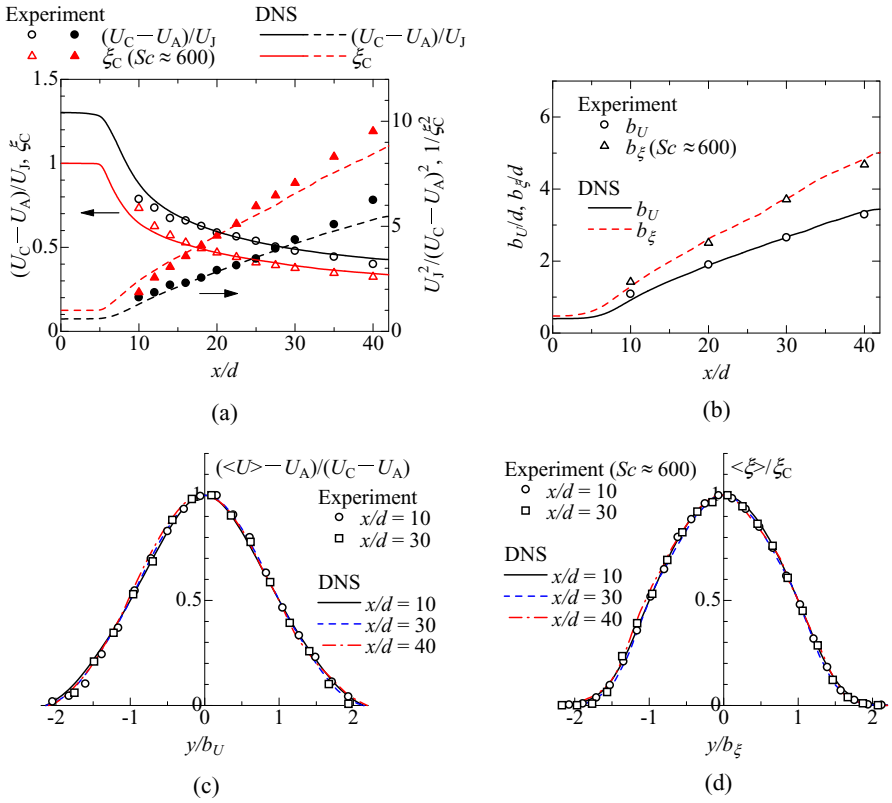

FIG. 3. Mean characteristics of streamwise velocity and mixture fraction. (a) Streamwise variation of mean streamwise velocity and mean mixture fraction on jet centerline. The closed symbols and dashed lines show $U_J^2/(U_C - U_A)^2$ and $1/\xi_C^2$. (b) Jet half-width (b_U, b_ξ) based on $\langle U\rangle - U_A$ and $\langle\xi\rangle$. (c) Cross-streamwise profile of mean streamwise velocity. (d) Cross-streamwise profile of mean mixture fraction. The present DNS results are compared with the experiment by Watanabe *et al.*[28–31]

Figure 7 shows the cross-streamwise turbulent mass flux $\langle v\gamma_P\rangle$ of the product P. Here, $\gamma_\alpha = \Gamma_\alpha - \langle\Gamma_\alpha\rangle$ is the fluctuating component of Γ_α. Because γ_A and γ_B are related to γ_P and $\xi' = \xi - \langle\xi\rangle$ by $\gamma_A = \Gamma_{A0}\xi' - \gamma_P$ and $\gamma_B = -\Gamma_{B0}\xi' - \gamma_P$ [Eqs. (7) and (8)], $\langle v\gamma_A\rangle$ and $\langle v\gamma_B\rangle$ are determined by $\langle v\gamma_P\rangle$ and the turbulent flux in the non-reactive flow. In the upstream region, $\langle\Gamma_P\rangle$ is large away from the jet centerline especially for the fast reaction (Fig. 5). Then, near the jet centerline, the

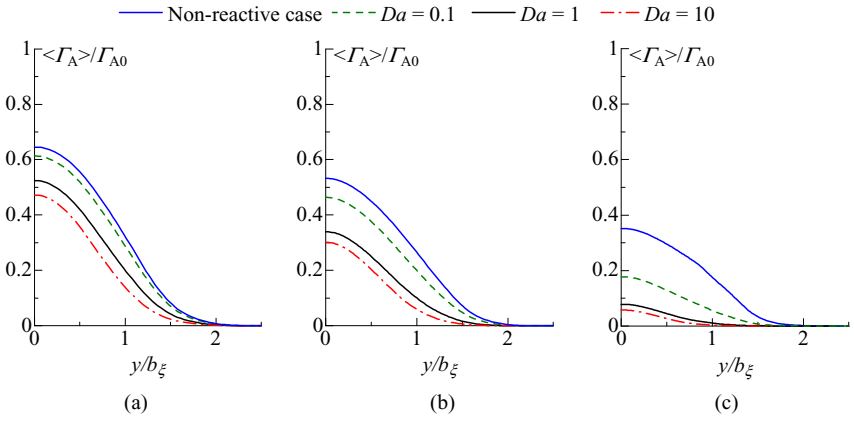

FIG. 4. Cross-streamwise profile of time-averaged concentration of reactant A. (a) $x/d = 10$. (b) $x/d = 15$. (c) $x/d = 38$.

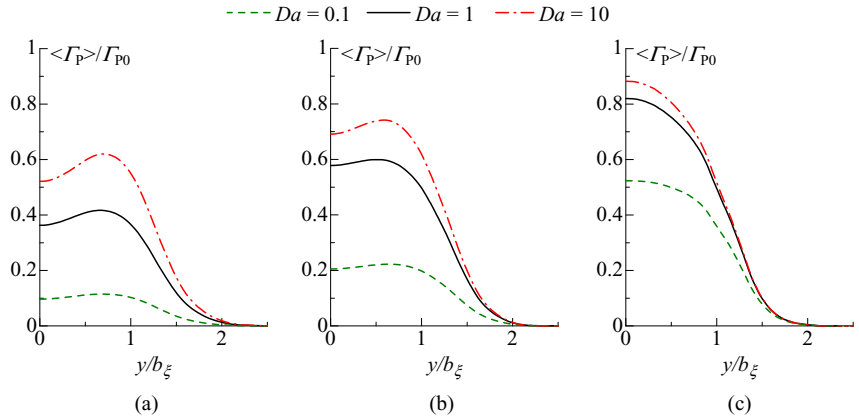

FIG. 5. Cross-streamwise profile of time-averaged concentration of product P. (a) $x/d = 10$. (b) $x/d = 15$. (c) $x/d = 38$.

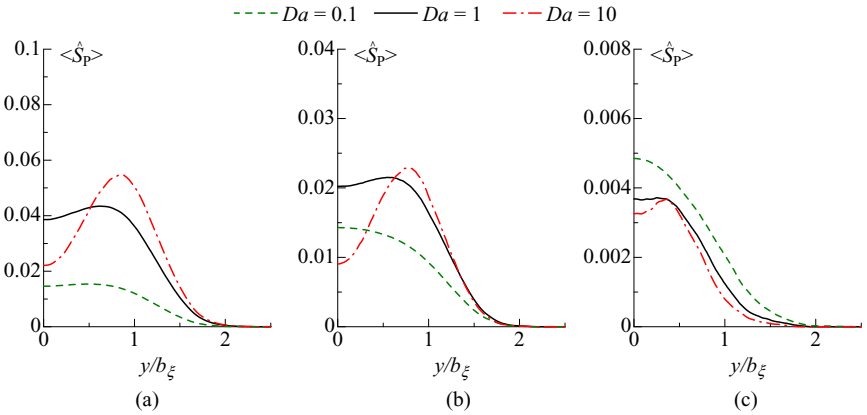

FIG. 6. Cross-streamwise profile of time-averaged chemical production rate of product P. (a) $x/d = 10$. (b) $x/d = 15$. (c) $x/d = 38$.

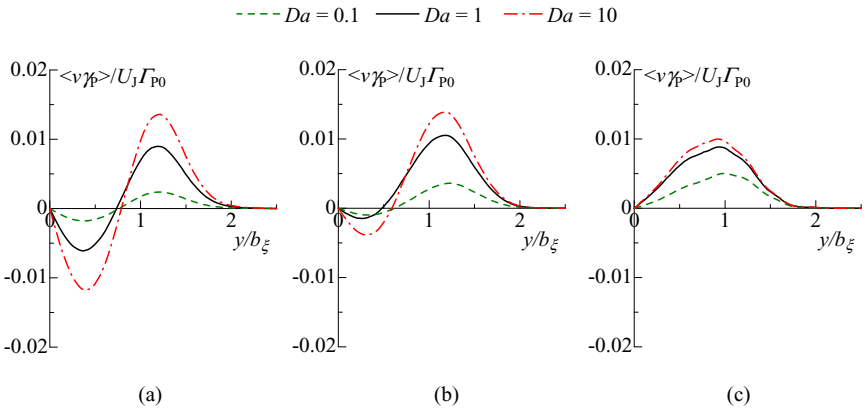

FIG. 7. Cross-streamwise profile of cross-streamwise turbulent mass flux of product P. (a) $x/d = 10$. (b) $x/d = 15$. (c) $x/d = 38$.

velocity toward the jet centerline, which causes negative v (in the region $y > 0$), is related to the large concentration of P (positive γ_P). Therefore, at $x/d = 10$ and 15, $\langle v\gamma_P \rangle$ is negative near the jet centerline. In contrast, in the outer region at $x/d = 10$ and 15 and the downstream region, $\langle \Gamma_P \rangle$ decreases to the y direction. Then, the outward velocity (positive v in the region $y > 0$) transports

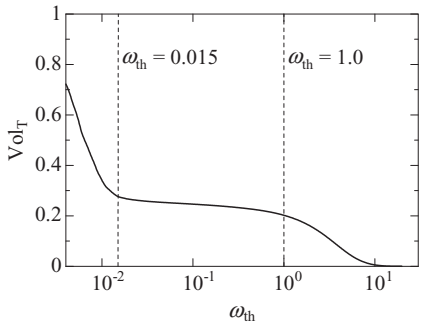

FIG. 8. Dependence of volume fraction of turbulent regions on interface detection threshold. $\mathrm{Vol_T}$ is calculated in the region $x/d \geq 10$.

a large amount of P, and $\langle v\gamma_P \rangle$ is positive in these regions. The magnitude of $\langle v\gamma_P \rangle$ increases with increasing Da because the increase in Γ_P due to the reaction enhances these effects.

B. Detection of the T/NT interface

The vorticity $\boldsymbol{\omega}$ is used to detect the T/NT interface, and the flow region where $|\boldsymbol{\omega}|b_U/U_C \geq \omega_{th}$ is detected as the turbulent region. The interface between the turbulent and non-turbulent regions is represented by the isosurface of $|\boldsymbol{\omega}|b_U/U_C = \omega_{th}$. As in Taveira *et al.*,[43] the threshold ω_{th} is determined from the relationship between ω_{th} and the volume fraction of the turbulent region ($\mathrm{Vol_T}$). Figure 8 shows $\mathrm{Vol_T}$ as a function of ω_{th}. As ω_{th} increases, the turbulent volume decreases, but $\mathrm{Vol_T}$ changes slowly for $0.015 \leq \omega_{th} \leq 1$. Thus, the interface location is almost independent of ω_{th} chosen from $0.015 \leq \omega_{th} \leq 1$, and $\omega_{th} = 0.7$ is used in this study. Note that the same threshold was also used by Bisset *et al.*[8]

The dependence of the reaction on the interface orientation is also investigated. Similar to previous studies on the T/NT interface,[23–25] we consider the three interface orientations (Fig. 9), which are distinguished by the unit vector normal to the T/NT interface, $\mathbf{n} = -\nabla\omega^2/|\nabla\omega^2|$. Here, $\omega^2/2$ is the enstrophy. The cross-streamwise edge is defined as the T/NT interface at which $\mathbf{n}$ is parallel to the cross-streamwise (y) direction. The leading edge is defined as the T/NT interface at which $\mathbf{n}$ points in the streamwise (x) direction, whereas the trailing edge is defined as that at which $\mathbf{n}$ is opposite to the x direction.

The conditional statistics conditioned on the distance from the T/NT interface[8] are analyzed using a procedure similar to that in previous works.[23–25] The local coordinate y_I, which is defined as shown in Fig. 9, is used to calculate the conditional statistics. The origin of y_I is located on the T/NT interface. Here, the height of the T/NT interface is represented by Y_I, and the y_I direction is normal to the T/NT interface. The turbulent fluid is on the side where $y_I < 0$. The conditional statistics conditioned on y_I are calculated for each interface orientation. The dependence of the conditional statistics on the interface orientation has been investigated by Bisset *et al.*[8] and Watanabe *et al.*,[23–25]

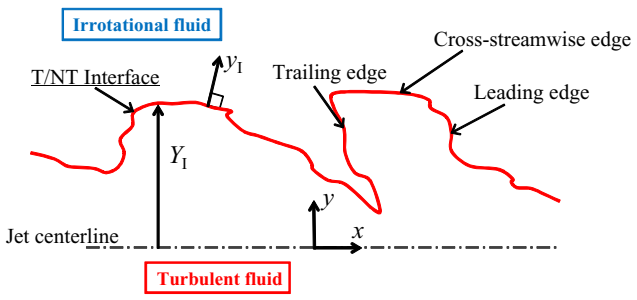

FIG. 9. Schematic of T/NT interface in jet flow and definition of interface orientation.

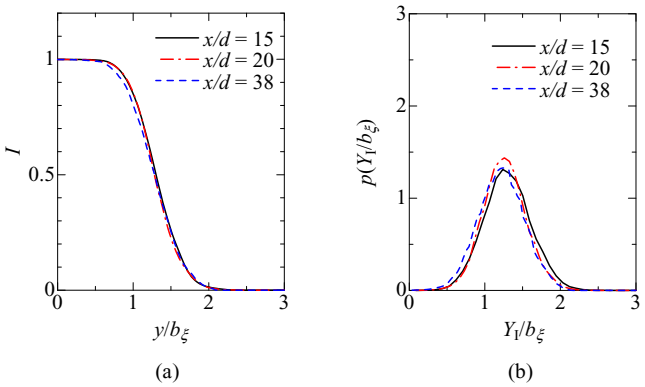

FIG. 10. Statistical properties of T/NT interface location. (a) Cross-streamwise profiles of intermittency factor. (b) Probability density function of T/NT interface height Y_I.

who accepted deviations of the interface orientation within $\pm 25^\circ$ for calculating the conditional statistics. We also use this criterion for choosing the interface used for calculating the conditional statistics. For the interface detected as the cross-streamwise edge, y_I is set to be parallel to the cross-streamwise direction. Similarly, for the interfaces detected as the leading and trailing edges, y_I is set to be parallel to the streamwise direction. The conditional statistics are calculated for the turbulent and non-turbulent sides of the T/NT interface. When the conditional statistics are calculated for a T/NT interface, other interfaces can appear on y_I near the T/NT interface. The characteristics of the flow field drastically vary near the T/NT interface, and the width of this variation is close to the Taylor microscale. Therefore, when other interfaces appear on y_I, the region within λ away from the other interfaces is not used for calculating the conditional statistics, where λ is the Taylor microscale $(\lambda_x + \lambda_y + \lambda_z)/3$. When $\omega_{th} = 0.7$ is used as the threshold, "pockets" of non-turbulent fluid are detected in the turbulent region. The T/NT interface associated with the pockets is not used for calculating the conditional statistics.

We analyze the statistical properties of the interface location. First, we calculate the intermittency factor I, which is defined as the fraction of time during which there is a turbulent fluid. The discriminant function D_T of the turbulent region is defined as

$$D_T = \begin{cases} 1 \text{ (turbulent region : } |\boldsymbol{\omega}| b_U / U_C \geq \omega_{th}) \\ 0 \text{ (non-turbulent region : } |\boldsymbol{\omega}| b_U / U_C < \omega_{th}). \end{cases} \tag{11}$$

Then, I is calculated from $I = \langle D_T \rangle$. Figure 10(a) shows the cross-streamwise profiles of I at different streamwise locations. The cross-streamwise profiles of I are independent of the streamwise location. The region of $|y/b_\xi| \leq 0.5$ is always turbulent, whereas both turbulent and non-turbulent fluids exist in the region of $0.5 \leq |y/b_\xi| \leq 2.2$. Figure 10(b) shows the probability density function (PDF) of the normalized interface height Y_I/b_ξ, which is also almost independent of the streamwise location. At $x/d = 38$, the mean T/NT interface height is $1.43 b_\xi$, and the rms value of the fluctuation of Y_I is $0.28 b_\xi$. The skewness and flatness of Y_I are -0.0569 and 3.00, respectively. Thus, the PDF of Y_I/b_ξ is similar to a Gaussian shape, which has been observed in previous studies.[8,17,36]

C. Visualization of the scalar field and T/NT interface

Figure 11 shows a snapshot of the mixture fraction field and T/NT interface on the x-y plane. The T/NT interface successfully divides the flow field into regions of $\xi \approx 0$ and $\xi > 0$, and the scalar interface between the jet and ambient fluids appears near the T/NT interface. Therefore, the diffusive scalar is often used to detect the T/NT interface in experiments[15–17] and large eddy simulations.[36] However, there exist a few non-turbulent fluids with a moderate mixture faction near the T/NT interface.

The chemical reaction rate of the fast chemical reaction is linked to the scalar dissipation rate of the mixture fraction $N = D(\nabla\xi \cdot \nabla\xi)$.[37] Figure 12(a) shows a snapshot of N on the x-y plane,

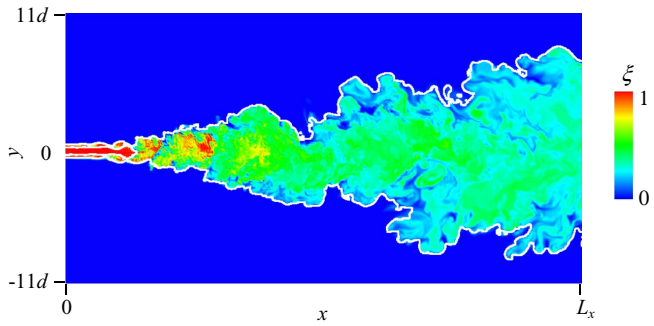

FIG. 11. Visualization of T/NT interface and mixture fraction. Thick white lines represent T/NT interface. Color contours represent value of mixture fraction ξ. Blue: $\xi = 0$, red: $\xi = 1$.

and Fig. 12(b) shows the T/NT interface and N. A comparison of the two figures shows that a large scalar dissipation rate appears along the T/NT interface. Therefore, the fast chemical reaction seems to occur near the T/NT interface.

Figure 13 shows Γ_{P} for $Da = 1$ and the T/NT interface on the x-y plane. The T/NT interface envelops the region where the product P exists, and most of P is contained in the turbulent region. The profile of Γ_{P} and the T/NT interface imply that the chemical reaction proceeds after the reactant B in the ambient flow is entrained into the turbulent region.

D. Conditional average of the vorticity magnitude

Figure 14 shows the conditional average of the normalized vorticity magnitude $|\boldsymbol{\omega}|b_U/U_{\mathrm{C}}$ near the cross-streamwise edge, leading edge, and trailing edge detected at different streamwise locations. The conditional average is represented by $\langle\ \rangle_{\mathrm{I}}$. The distance from the T/NT interface y_{I}

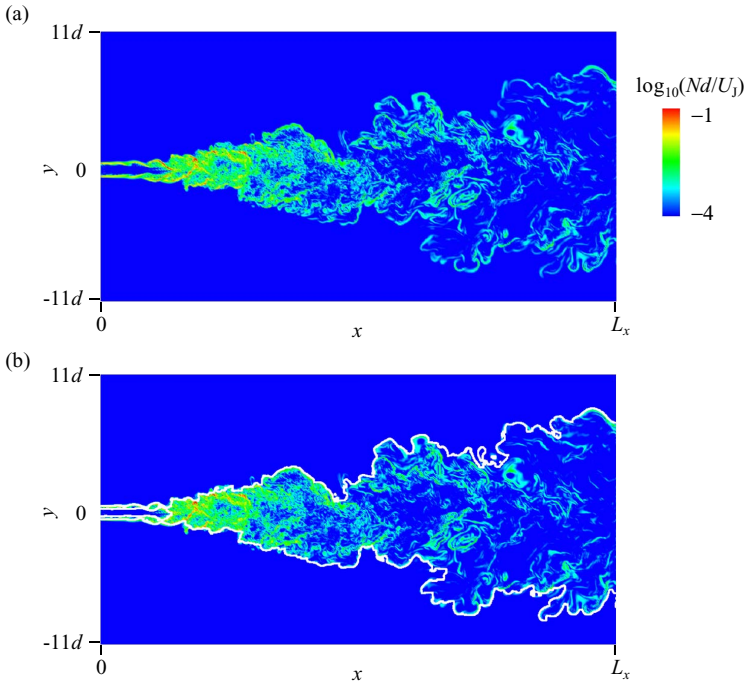

FIG. 12. Visualization of T/NT interface and scalar dissipation rate of mixture fraction. (a) Scalar dissipation rate. (b) Relationship between scalar dissipation rate and T/NT interface. Thick white lines represent T/NT interface. Color contours represent value of scalar dissipation rate, $\log_{10}(Nd/U_{\mathrm{J}})$. Blue: $\log_{10}(Nd/U_{\mathrm{J}}) = -4$, red: $\log_{10}(Nd/U_{\mathrm{J}}) = -1$.

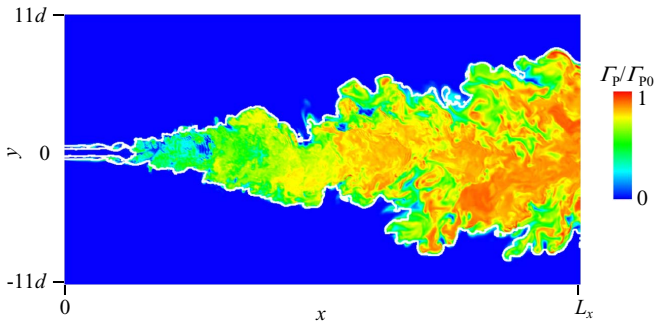

FIG. 13. Visualization of T/NT interface and concentration of product P ($Da = 1$). Thick white lines represent T/NT interface. Color contours represent value of concentration of product P, Γ_P. Blue: $\Gamma_P/\Gamma_{P0} = 0$, red: $\Gamma_P/\Gamma_{P0} = 1$.

is normalized by λ on the jet centerline because the Taylor microscale is almost independent of the cross-streamwise location in the turbulent region.[13] A sharp jump in $\langle|\boldsymbol{\omega}|b_U/U_C\rangle_I$ can be observed near the T/NT interface. Near the cross-streamwise edge detected at $x/d = 38$, $\langle|\boldsymbol{\omega}|b_U/U_C\rangle_I$ reaches a peak value at $y_I/\lambda \approx -0.64$. As in many figures in this paper, the vertical broken line indicates $y_I/\lambda = -0.64$. Figure 14 shows that the width of the jump in $\langle|\boldsymbol{\omega}|b_U/U_C\rangle_I$ is almost independent of the interface orientation and the streamwise location of the interface. This width of the vorticity jump is similar to the DNS results for a temporally developing planar jet.[13] The vorticity magnitudes in the turbulent and non-turbulent regions differ significantly, and are adjusted in the region of $-0.64 \le y_I/\lambda \le 0$ so that the vorticity varies continuously across the T/NT interface. For simplicity, the region where a sharp jump in $\langle|\boldsymbol{\omega}|b_U/U_C\rangle_I$ appears is referred to as the adjustment layer hereafter.

Figure 15 compares the conditional mean enstrophy among the cross-streamwise, leading, and trailing edges. The enstrophy level strongly depends on the interface orientation, and is largest and smallest near the cross-streamwise and trailing edges, respectively. Although $\langle\omega^2/2\rangle_I$ sharply increases from the non-turbulent region to the turbulent region, the slope of this increase is small near the trailing edge.

E. Statistical properties of the concentrations of the reactive species in the turbulent region

The time averages of the concentrations and reaction rate strongly depend on the outer intermittency because the unmixed ambient fluid is used to calculate the statistics. To investigate the characteristics of the reactive scalar field in the turbulent region, we analyze the average in the

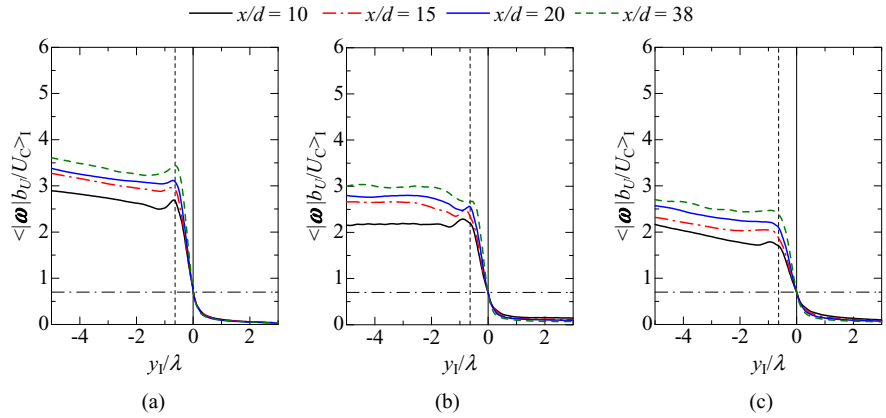

FIG. 14. Conditional average of normalized vorticity magnitude near (a) cross-streamwise edge, (b) leading edge, and (c) trailing edge. Horizontal dashed-dotted lines show the threshold $\omega_{th} = 0.7$ and vertical broken lines show $y_I/\lambda = -0.64$.

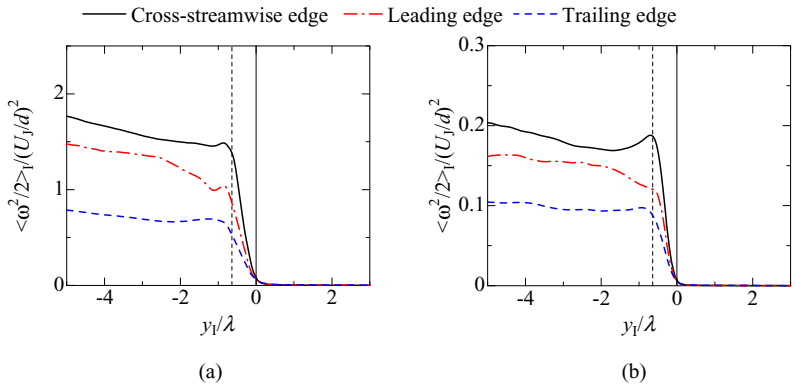

FIG. 15. Conditional mean enstrophy near cross-streamwise, leading, and trailing edges. (a) $x/d = 15$. (b) $x/d = 38$.

turbulent region. The average of variable f in the turbulent region is defined as[38]

$$\langle f \rangle_T = \frac{\langle D_T f \rangle}{I}. \tag{12}$$

Figure 16 shows the cross-streamwise profile of $\langle \Gamma_A \rangle_T$ at $x/d = 10$, 15, and 38. The average of Γ_A in the turbulent region is large near the jet centerline because the reactant A is supplied from the jet flow. In the non-reactive flow, $\langle \Gamma_A \rangle_T$ has a non-zero value even in the outer region of the jet flow. At $x/d = 38$, $\langle \Gamma_A \rangle_T$ for $Da = 1$ and 10 is nearly zero in the region of $y/b_\xi > 1$. Thus, most of A has reacted, and the chemical reaction reaches the equilibrium state, in which one of the reactants is completely consumed by the reaction. Figure 17 shows the cross-streamwise profile of $\langle \Gamma_P \rangle_T$, which differs significantly from the time-averaged value in Fig. 5. The change in $\langle \Gamma_P \rangle_T$ in the cross-streamwise direction is small. At $x/d = 10$ and 15, $\langle \Gamma_P \rangle_T$ for $Da = 0.1$ is independent of the cross-streamwise location. However, $\langle \Gamma_P \rangle_T$ for $Da = 1$ and 10 is large away from the jet centerline at $x/d = 10$. In the downstream region (at $x/d = 38$), $\langle \Gamma_P \rangle_T$ near the jet centerline is large. Thus, the product P exists in the entire turbulent region.

Figure 18 shows the cross-streamwise profile of $\langle \hat{S}_P \rangle_T$. At $x/d = 10$ and 15, $\langle \hat{S}_P \rangle_T$ for $Da = 10$ becomes large away from the jet centerline. $\langle \hat{S}_P \rangle_T$ for $Da = 0.1$ and 1 is almost independent of the cross-streamwise location at $x/d = 10$. Thus, in the upstream region, the fast chemical reaction occurs mainly away from the jet centerline, whereas the slow chemical reaction occurs in the entire turbulent region. At $x/d = 38$, the chemical production rate becomes small in the cross-streamwise

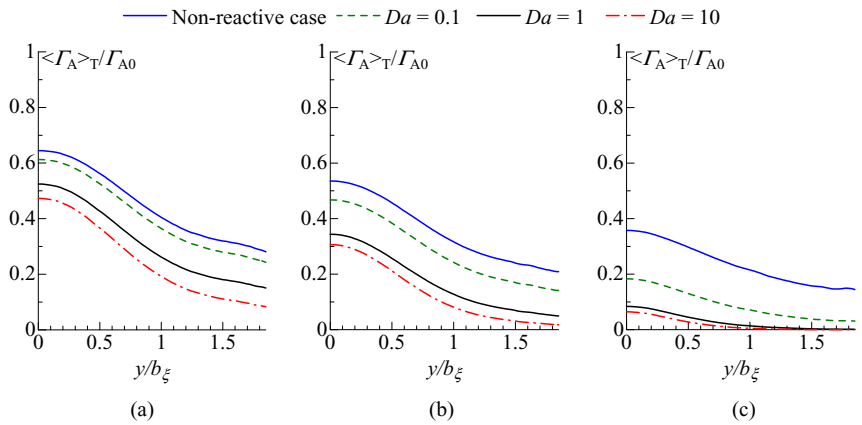

FIG. 16. Cross-streamwise profile of mean concentration of reactant A in turbulent region. (a) $x/d = 10$. (b) $x/d = 15$. (c) $x/d = 38$.

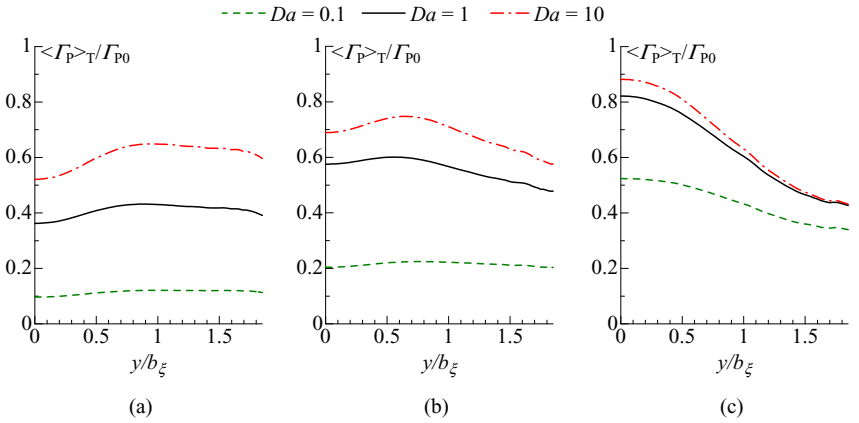

FIG. 17. Cross-streamwise profile of mean concentration of product P in turbulent region. (a) $x/d = 10$. (b) $x/d = 15$. (c) $x/d = 38$.

direction because most of the reactant A has reacted in the outer region at $x/d = 38$ before it reaches this region.

F. Conditional mean concentrations of the reactive species

Figures 19 and 20 show the conditional mean concentration of the reactive species $\langle \Gamma_\alpha \rangle_I$ for (a) $Da = 0.1$, (b) $Da = 1$, and (c) $Da = 10$ near the cross-streamwise edge detected at $x/d = 15$ and 38, respectively. These figures show that $\langle \Gamma_\alpha \rangle_I$ differs significantly between the turbulent and non-turbulent regions, and changes sharply in the adjustment layer. The width of the jump in $\langle \Gamma_\alpha \rangle_I$ is similar to that in $\langle |\boldsymbol{\omega}| b_U / U_C \rangle_I$ and is almost independent of the chemical species and Damköhler number. At $x/d = 38$, most of the reactant A near the interface has reacted for $Da = 1$ and 10, and $\langle \Gamma_A \rangle_I$ is nearly zero. Therefore, the chemical reaction for $Da = 1$ and 10 reaches the equilibrium state near the T/NT interface in the downstream region. Figure 10(b) shows that the T/NT interface appears in the region of $0.5 \leq y/b_\xi \leq 2.2$. Therefore, the reactant A for $Da = 1$ and 10 in the turbulent region exists only near the jet centerline, which is far away from the T/NT interface, and the chemical reaction for $Da = 1$ and 10 in the outer region is in the equilibrium state [Fig. 16(c)]. The reactant B is supplied from the ambient flow and entrained into the turbulent region. Therefore, $\langle \Gamma_B \rangle_I$ in the turbulent region near the interface increases from $x/d = 15$ to 38 in the non-reactive case (Figs. 19 and 20). For $Da = 0.1$, $\langle \Gamma_B \rangle_I$ in the turbulent region decreases slightly from

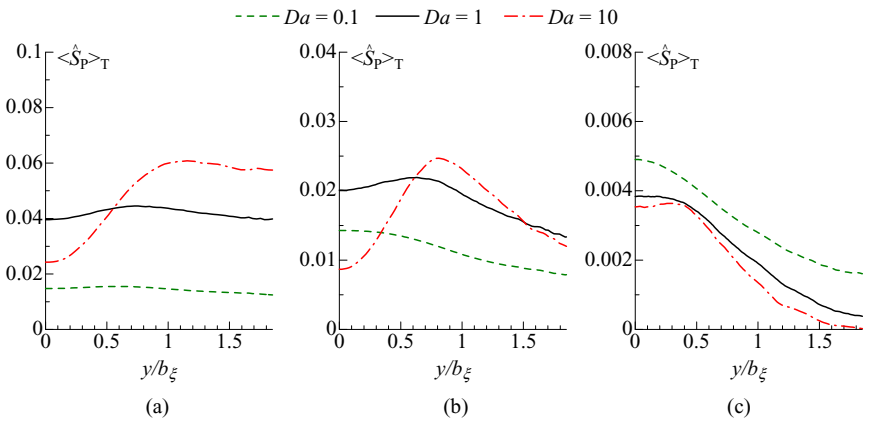

FIG. 18. Cross-streamwise profile of mean chemical production rate of product P in turbulent region. (a) $x/d = 10$. (b) $x/d = 15$. (c) $x/d = 38$.

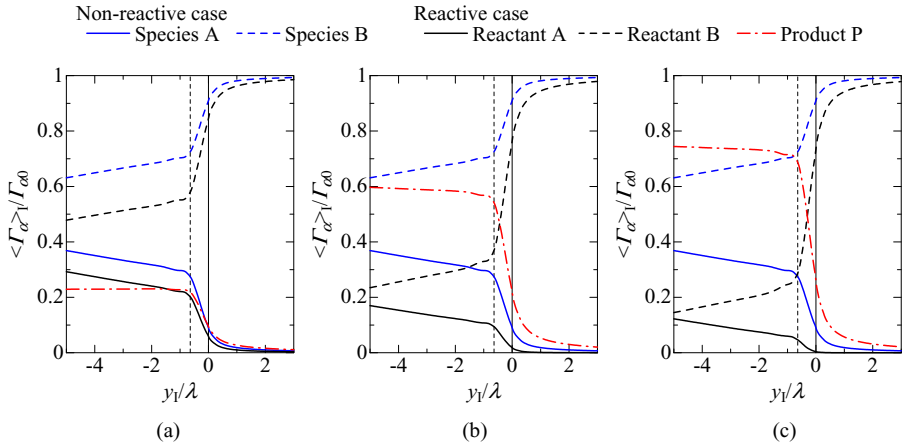

FIG. 19. Conditional mean concentration of reactive species near cross-streamwise edge detected at $x/d = 15$. (a) $Da = 0.1$. (b) $Da = 1$. (c) $Da = 10$.

$x/d = 15$ to 38 because the chemical reaction consumes it. In contrast, $\langle \Gamma_B \rangle_I$ for $Da = 1$ and 10 increases from $x/d = 15$ to 38 because the reactant B is entrained into the turbulent region after most of the reactant A has reacted. In the adjustment layer, $\langle \Gamma_P \rangle_I$ increases from the non-turbulent region toward the turbulent region and almost reaches the mean value in the turbulent region (Fig. 17). The concentration of P is small in the non-turbulent region, and most of P is contained in the turbulent region.

Figure 21 compares $\langle \xi \rangle_I$ among the three different interface orientations. The mixture fraction smaller (larger) than ξ_S means that the reactant A (B) is deficient. It is found that $\langle \xi \rangle_I$ tends to be smaller than ξ_S near the interface, and is smallest near the trailing edge. Thus, the reactant A tends to be deficient especially near the trailing edge. This is the reason that concentration of A is close to zero for $Da = 1$ and 10 near the interface in the downstream region. $\langle \xi \rangle_I$ shows the large difference between the turbulent and non-turbulent regions, $\langle \xi \rangle_I$ has a non-zero value in the non-turbulent region near the interface. Thus, the reaction can occur in both turbulent and non-turbulent regions. However, the reaction mainly occurs in the turbulent region because the non-turbulent fluids contain only small amount of A.

We compare $\langle \Gamma_P \rangle_I$ for the different interface orientations in Figs. 22 and 23. $\langle \Gamma_P \rangle_I$ is almost constant in the turbulent region near the T/NT interface at $x/d = 15$. At $x/d = 15$, $\langle \Gamma_P \rangle_I$ for $Da = 1$

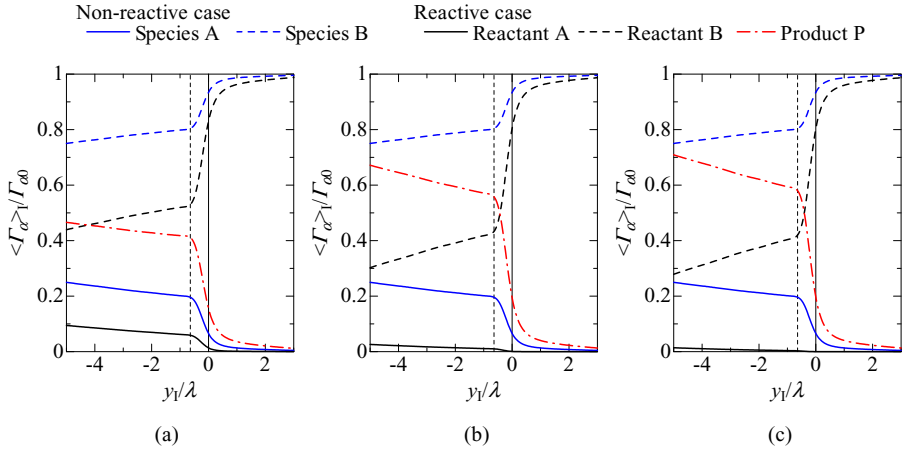

FIG. 20. Conditional mean concentration of reactive species near cross-streamwise edge detected at $x/d = 38$. (a) $Da = 0.1$. (b) $Da = 1$. (c) $Da = 10$.

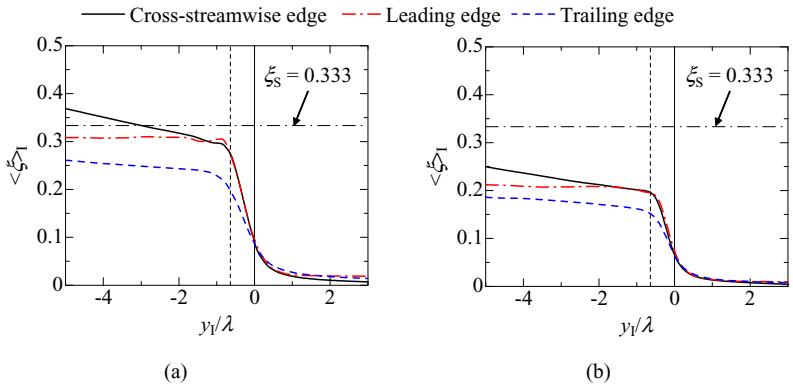

FIG. 21. Conditional mean mixture fraction near cross-streamwise, leading, and trailing edges. (a) $x/d = 15$. (b) $x/d = 38$. The stoichiometric value of mixture fraction $\xi_S = 0.333$ is shown by horizontal dashed-dotted lines.

and 10 near the trailing edge is small compared with the value near the cross-streamwise and leading edges. At $x/d = 38$, $\langle \Gamma_P \rangle_I$ near the trailing edge is smaller for all Da. These results show that the difference in $\langle \Gamma_P \rangle_I$ between the trailing edge and the other interfaces becomes large as Da increases. Figure 24 shows $\langle \Gamma_A \rangle_I$ at $x/d = 15$. Γ_A is related to ξ by Eq. (7). Therefore, the concentration of A is very small near the interface because of the small mixture fraction and the consumption by the reaction. $\langle \Gamma_A \rangle_I$ is small especially near the trailing edge and this is caused by the small mixture fraction near the trailing edge (Fig. 21).

G. The chemical production rate near the T/NT interface

The chemical production rate near the T/NT interface is analyzed here. First, we investigate the scalar dissipation rate N near the T/NT interface. Figure 25 shows the conditional average of N, $\langle N \rangle_I$. $\langle N \rangle_I$ has a large peak near the T/NT interface. A similar profile of $\langle N \rangle_I$ was observed in a temporally developing planar jet.[39] In addition, $\langle N \rangle_I$ is the smallest near the trailing edge among the three interface orientations.

Figure 26 shows $\langle \hat{S}_P \rangle_I$ near the interface detected at $x/d = 15$. $\langle \hat{S}_P \rangle_I$ for $Da = 0.1$ gradually increases from the non-turbulent region toward the turbulent region. In contrast, a peak value of $\langle \hat{S}_P \rangle_I$ appears near the T/NT interface for the chemical reaction with $Da = 1$ and 10. These peak values of $\langle \hat{S}_P \rangle_I$ appear in the region where $\langle N \rangle_I$ is large. $\langle \hat{S}_P \rangle_I$ for $Da = 0.1$ and 1 is almost constant

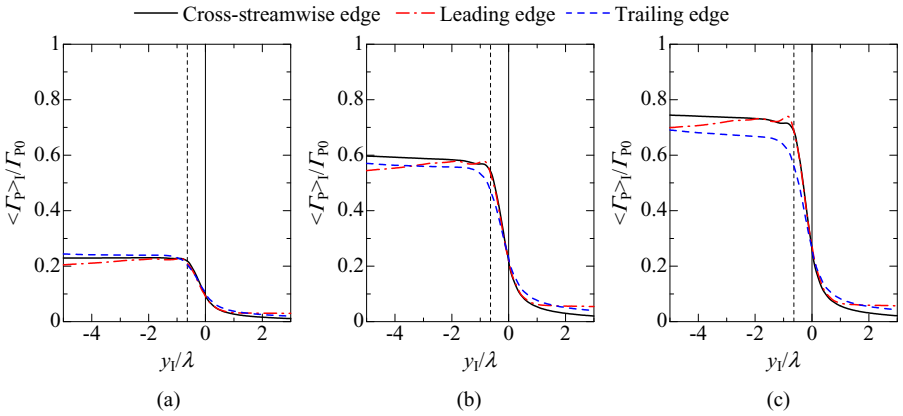

FIG. 22. Conditional mean concentration of product P for (a) $Da = 0.1$, (b) $Da = 1$, and (c) $Da = 10$ near cross-streamwise, leading, and trailing edges detected at $x/d = 15$.

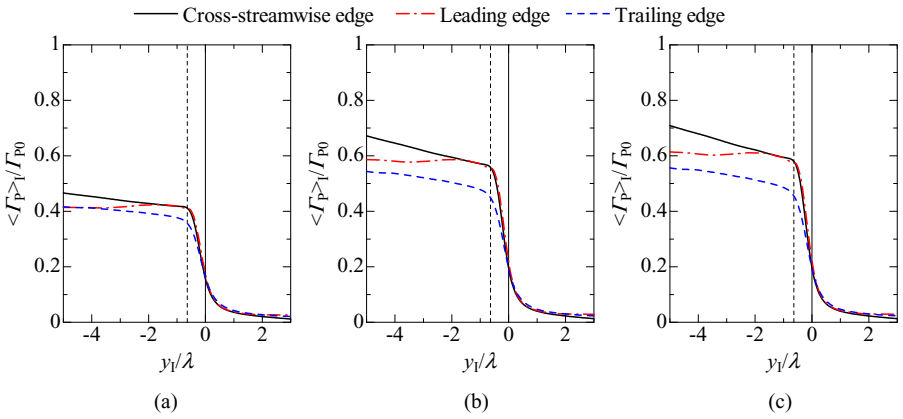

FIG. 23. Conditional mean concentration of product P for (a) $Da = 0.1$, (b) $Da = 1$, and (c) $Da = 10$ near cross-streamwise, leading, and trailing edges detected at $x/d = 38$.

in the turbulent region. Figure 27 shows $\langle \hat{S}_P \rangle_I$ at $x/d = 38$. At $x/d = 38$, most of the reactant A for $Da = 1$ and 10 has reacted near the interface (Fig. 20). Therefore, the production rate becomes small as Da increases. $\langle N \rangle_I$ is large in the adjustment layer near the T/NT interface detected at $x/d = 38$ [Fig. 25(b)]. However, a peak value of $\langle \hat{S}_P \rangle_I$ is much smaller than its value at $x/d = 15$. Figure 27 shows that the production rate increases from the T/NT interface toward the deep interior of the turbulent region. The mean production rate in the turbulent region $\langle \hat{S}_P \rangle_T$ [Fig. 18(c)] also shows that the production rate in the downstream region becomes large near the jet centerline. Thus, in the downstream region, the chemical reaction occurs mainly in the turbulent region away from the T/NT interface. Figures 26 and 27 show that the production rate is smallest near the trailing edge among the three interface orientations. The difference in the production rate among the three interface orientations becomes large as Da increases. Thus, the characteristics of the T/NT interface greatly affect the fast reaction. The mechanism of mixing and chemical reactions near the T/NT interface is expected to be crucial for modeling turbulent flows with fast reactions.

$\langle \hat{S}_P \rangle_I$ can be decomposed into the product of the conditional mean concentrations and the conditional correlation of the fluctuating components of concentrations (concentration correlation):

$$\langle \hat{S}_P \rangle_I = Da \langle \hat{\Gamma}_A \hat{\Gamma}_B \rangle_I = Da \langle \hat{\Gamma}_A \rangle_I \langle \hat{\Gamma}_B \rangle_I + Da \langle \hat{\gamma}'_A \hat{\gamma}'_B \rangle_I, \tag{13}$$

$$= Da \langle \hat{\Gamma}_A \rangle_I \langle \hat{\Gamma}_B \rangle_I (1 + I_{SI}). \tag{14}$$

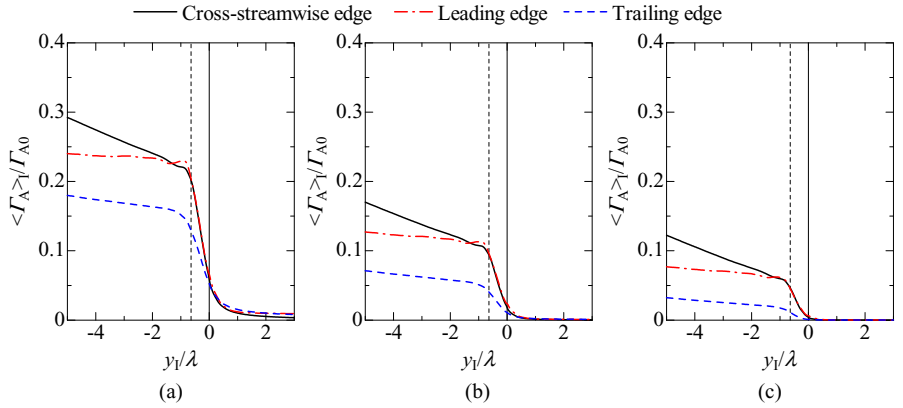

FIG. 24. Conditional mean concentration of reactant A for (a) $Da = 0.1$, (b) $Da = 1$, and (c) $Da = 10$ near the cross-streamwise, leading, and trailing edges detected at $x/d = 15$.

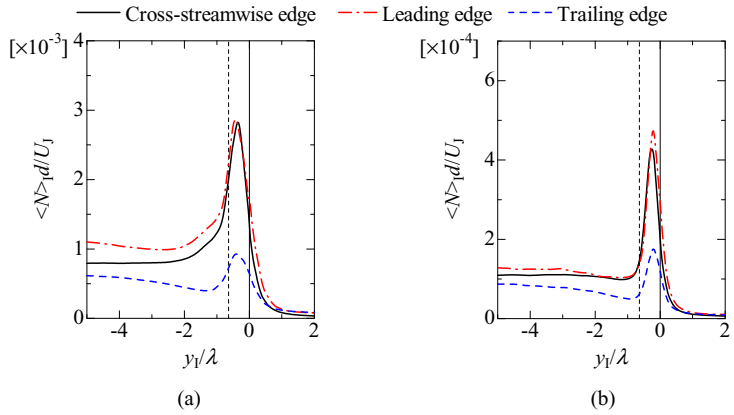

FIG. 25. Conditional mean scalar dissipation rate N near T/NT interface detected at (a) $x/d = 15$ and (b) $x/d = 38$. N is normalized by d and U_J.

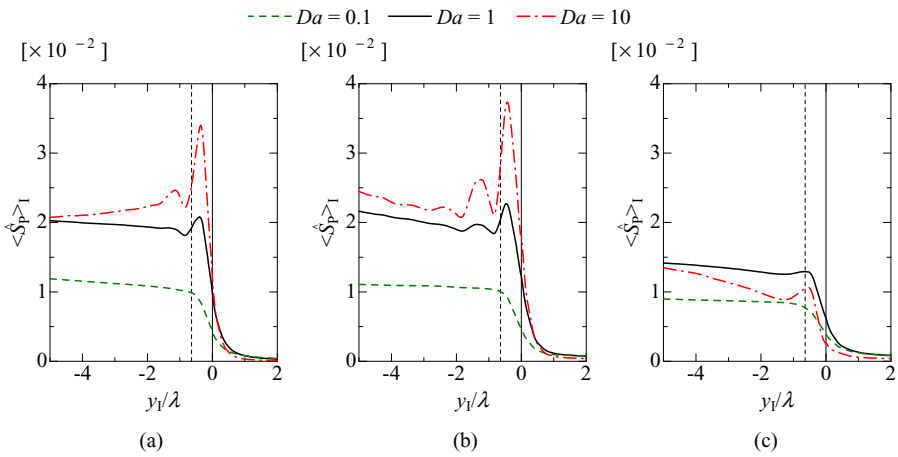

FIG. 26. Conditional mean production rate of product P near (a) cross-streamwise edge, (b) leading edge, and (c) trailing edge detected at $x/d = 15$.

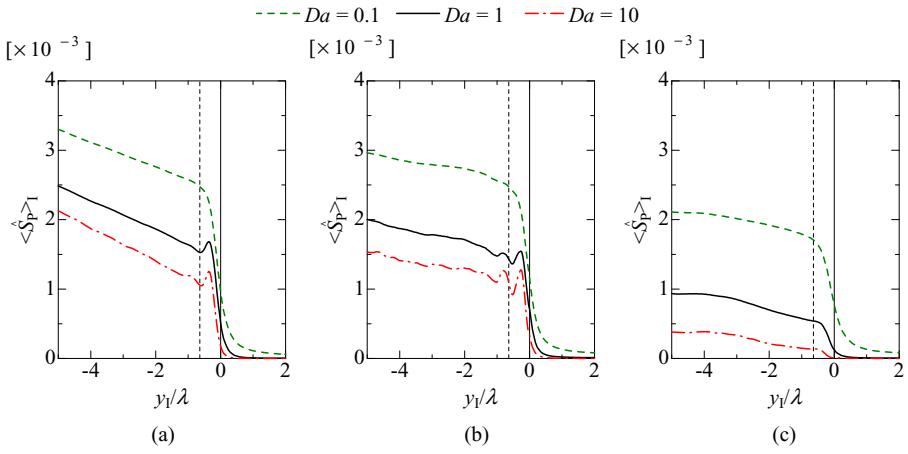

FIG. 27. Conditional mean production rate of product P near (a) cross-streamwise edge, (b) leading edge, and (c) trailing edge detected at $x/d = 38$.

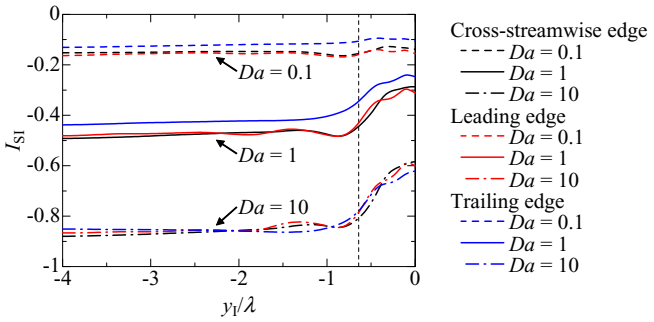

FIG. 28. Conditional segregation intensity in turbulent region near T/NT interface at $x/d = 15$.

Here, $\gamma'_\alpha = \Gamma_\alpha - \langle\Gamma_\alpha\rangle_I$ is the fluctuating component from the conditional mean concentration, and $\hat{\gamma}'_\alpha = \gamma'_\alpha/\Gamma_{\alpha 0}$. The conditional segregation intensity I_{SI} is defined by

$$I_{SI} = \frac{\langle\gamma'_A\gamma'_B\rangle_I}{\langle\Gamma_A\rangle_I\langle\Gamma_B\rangle_I}. \tag{15}$$

Similar to the segregation intensity defined by the time-averaged concentration correlation,[40–42] the conditional segregation intensity has a negative value between -1 and 0. The segregation intensity is the measure of the unmixedness of the two reactants. When two reactants do not coexist and are fully segregated, $I_{SI} = -1$. With the mixing of these two reactants, the segregation intensity approaches 0. When the two reactants are completely and ideally mixed, $I_{SI} = 0$. From Eq. (14), we can see that the unmixedness represented by negative I_{SI} suppresses the mean reaction rate and $\langle\hat{S}_P\rangle_I$ is determined by the conditional mean concentration and the segregation intensity.

Figure 28 shows I_{SI} in the turbulent region near the interface at $x/d = 15$. The previous experiment showed that the segregation intensity decreases owing to the reaction because the chemical product causes the two reactants to be segregated.[41] This is also seen in the conditional segregation intensity near the interface. The chemical reaction makes I_{SI} small, and I_{SI} decreases as Da increases. For $Da = 0.1$ and 1, I_{SI} is small near the cross-streamwise and leading edge. For $Da = 10$, I_{SI} is less sensitive to the interface orientation. Thus, the mixing of the reactants is close to the ideal state near the trailing edge. These results show that the small $\langle\hat{S}_P\rangle_I$ near the trailing edge is not caused by the mixing state because the unmixedness suppresses $\langle\hat{S}_P\rangle_I$ especially near the cross-streamwise and leading edges. Then, we can conclude that the small reaction rate near the trailing edge is caused by small concentration of the deficient reactant A (small $\langle\Gamma_A\rangle_I$). Thus, the mean concentrations of the reactants are more important than the mixing state in the dependence of the reaction on the interface orientation.

H. The reactive scalar transport near the T/NT interface

We analyze the reactive scalar transport near the T/NT interface. In this analysis, the movement of the T/NT interface should be taken into account. The velocity of the T/NT interface movement can be divided into two components. One is the velocity of the fluid at which the interface is located ($\mathbf{U}$), and the other is the velocity of the T/NT interface movement relative to the velocity of the fluid, which is referred to as the local entrainment velocity $\mathbf{V}^P$. The local entrainment velocity represents the velocity of the interface propagation. Hence, the velocity of the T/NT interface movement $\mathbf{U}^I$ is represented by $\mathbf{U}^I = \mathbf{U} + \mathbf{V}^P$. According to Holzner and Lüthi,[20] when the T/NT interface is defined as the isosurface of the enstrophy ($\omega^2/2$), $\mathbf{V}^P$ is represented by

$$\mathbf{V}^P = v_n\mathbf{n} = v_n\frac{-\nabla\omega^2}{|\nabla\omega^2|}, \tag{16}$$

$$v_n = \frac{2\omega_i\omega_j S_{ij}}{|\nabla\omega^2|} + \frac{2\nu\omega_i\nabla^2\omega_i}{|\nabla\omega^2|}, \tag{17}$$

where $S_{ij} = (\partial U_i/\partial x_j + \partial U_j/\partial x_i)/2$ is the rate of strain tensor and v_n is the local entrainment velocity component normal to the T/NT interface. Here, v_n is defined as positive when the T/NT interface propagates toward the non-turbulent region.

According to Watanabe *et al.*,[25] we introduce a local coordinate system moving with the T/NT interface, which is represented by $\mathbf{x}^I$. The origin of the local coordinate system is located on the T/NT interface, and moves with a speed of $\mathbf{U}^I$. The coordinate system $\mathbf{x}$ whose origin is located at the jet inlet is referred to as a fixed coordinate system hereafter. We consider the coordinate transformation from the fixed coordinate system $(\mathbf{x}, t)$ to the local coordinate system $(\mathbf{x}^I, t')$. Here, t and t' represent time in the coordinate systems. The location represented by $\mathbf{x} = \mathbf{x}_0^I$ in the fixed coordinate system is assumed to be located on the T/NT interface, and is used as the origin of the local coordinate system. Then, the local coordinate system for the origin $\mathbf{x}_0^I$ is related to the fixed coordinate system by

$$\mathbf{x} = \mathbf{x}_0^I + \mathbf{x}^I, \tag{18}$$

$$t = t'. \tag{19}$$

Because the origin of the local coordinate system moves with $\mathbf{U}^I$, we can obtain the following relationship from Eq. (18):

$$\frac{\partial \mathbf{x}_0^I}{\partial t} = -\frac{\partial \mathbf{x}^I}{\partial t} = \mathbf{U}^I. \tag{20}$$

Then, the derivative of the variable $f = f(\mathbf{x}^I, t')$ with respect to x_i is written as follows:

$$\frac{\partial f}{\partial x_i} = \frac{\partial f}{\partial t'}\frac{\partial t'}{\partial x_i} + \frac{\partial f}{\partial x_j^I}\frac{\partial x_j^I}{\partial x_i} = \frac{\partial f}{\partial x_i^I}. \tag{21}$$

Here, x_i and x_i^I are the i direction components of $\mathbf{x}$ and $\mathbf{x}^I$, respectively. Similarly, by using Eq. (20), we can represent the derivative of $f = f(\mathbf{x}^I, t')$ with respect to t as follows:

$$\frac{\partial f}{\partial t} = \frac{\partial f}{\partial t'}\frac{\partial t'}{\partial t} + \frac{\partial f}{\partial x_i^I}\frac{\partial x_i^I}{\partial t} = \frac{\partial f}{\partial t'} - U_i^I\frac{\partial f}{\partial x_i^I}. \tag{22}$$

Here, U_i^I is the i direction component of $\mathbf{U}^I$. By using Eqs. (21) and (22), the Lagrangian derivative of f at $\mathbf{x} = \mathbf{x}_0^I + \mathbf{x}^I$ can be represented in the local coordinate system $(\mathbf{x}^I, t')$ as follows:

$$\frac{Df}{Dt} = \frac{\partial f}{\partial t} + U_i(\mathbf{x}^I + \mathbf{x}_0^I)\frac{\partial f}{\partial x_i}, \tag{23}$$

$$= \frac{\partial f}{\partial t'} - U_i^I\frac{\partial f}{\partial x_i^I} + U_i(\mathbf{x}^I + \mathbf{x}_0^I)\frac{\partial f}{\partial x_i^I}, \tag{24}$$

$$= \frac{\partial f}{\partial t'} + \left(U_i(\mathbf{x}^I + \mathbf{x}_0^I) - U_i^I\right)\frac{\partial f}{\partial x_i^I}. \tag{25}$$

Then, the transport equation of the concentration of species α in the local coordinate system is derived from Eq. (25):

$$\frac{\partial \Gamma_\alpha}{\partial t'} + \left(U_i(\mathbf{x}^I + \mathbf{x}_0^I) - U_i^I\right)\frac{\partial \Gamma_\alpha}{\partial x_i^I} = D\frac{\partial^2 \Gamma_\alpha}{\partial x_i^I \partial x_i^I} + S_\alpha. \tag{26}$$

This equation is also represented in the following form using Eq. (21):

$$\frac{\partial \Gamma_\alpha}{\partial t'} = -\left(\mathbf{U}(\mathbf{x}^I + \mathbf{x}_0^I) - \mathbf{U}^I\right)\cdot\nabla\Gamma_\alpha + D\nabla^2\Gamma_\alpha + S_\alpha. \tag{27}$$

This form is useful because we can evaluate the spatial derivative in the fixed coordinate. The first term on the right-hand side in Eq. (27) represents the transport of Γ_α due to the relative velocity $(\mathbf{U} - \mathbf{U}^I)$ in the local coordinate system. The second term is the molecular diffusion term, and the third term is the chemical source term. The relative velocity can be written by

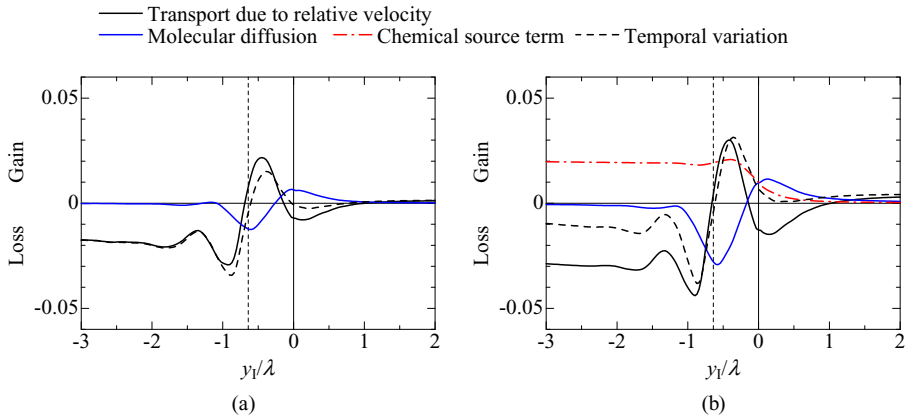

FIG. 29. Conditional average of scalar transport equation in local coordinate system near cross-streamwise edge detected at $x/d = 15$. (a) Species A (non-reactive case). (b) Product P ($Da = 1$). The transport equation is normalized by d, U_J, and $\Gamma_{\alpha 0}$.

$\mathbf{U}(\mathbf{x}^I + \mathbf{x}_0^I) - \mathbf{U}^I = \mathbf{U}(\mathbf{x}^I + \mathbf{x}_0^I) - \mathbf{U}(\mathbf{x}_0^I) - \mathbf{V}^P$, and is determined by the fluid velocity difference $\mathbf{U}(\mathbf{x}^I + \mathbf{x}_0^I) - \mathbf{U}(\mathbf{x}_0^I)$ and the propagation velocity $\mathbf{V}^P$

Figure 29(a) shows the conditional average of Eq. (27) for Γ_A in the non-reactive case near the cross-streamwise edge detected at $x/d = 15$. Figure 29(b) shows the results for Γ_P for $Da = 1$. The conditional averages of the molecular diffusion terms for A and P have positive and negative values near the T/NT interface. These profiles show that Γ_A and Γ_P in the turbulent region are transferred toward the non-turbulent region by the molecular diffusion. We have also confirmed that the role of the molecular diffusion is independent of the interface orientations. The product P is produced by the chemical reaction even in the non-turbulent region near the T/NT interface. Thus, the molecular diffusion term contributes to the increase in Γ_A in the non-turbulent region, and the molecular diffusion and chemical source terms contribute to the increase in Γ_P in the non-turbulent region. However, $\langle \Gamma_A \rangle_I$ and $\langle \Gamma_P \rangle_I$ (Figs. 19 and 20) show that only small amounts of A and P exist in the non-turbulent region near the T/NT interface. The reason is the negative value of the transport due to the relative velocity ($-0.2 \leq y_I/\lambda \leq 1$), which almost balances with the sum of molecular diffusion and chemical source terms. The role of the relative velocity is considered in detail below.

In Fig. 29, we can clearly see that the transport due to the relative velocity has an important role in both turbulent and non-turbulent regions near the interface. Figure 30 shows the interface normal component of the first term in Eq. (27) for Γ_A in the non-reactive case and Γ_P for $Da = 1$. Near the cross-streamwise edge, the conditional profile of the normal component is close to the total

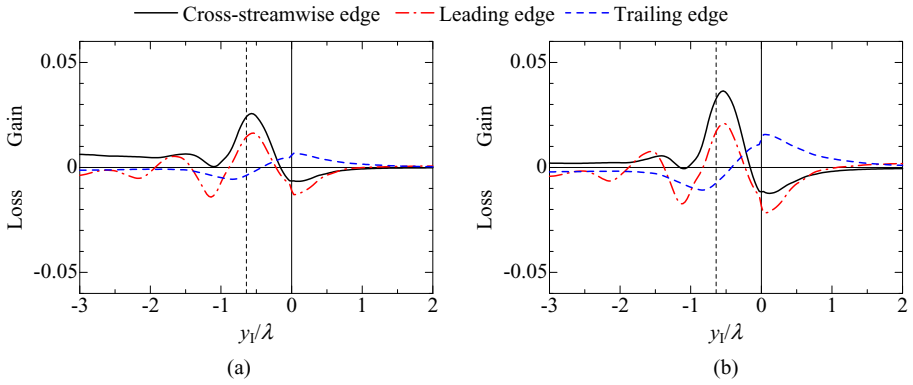

FIG. 30. Conditional average of transport term due to relative velocity in interface normal direction near cross-streamwise, leading, and trailing edges. (a) Species A (non-reactive case). (b) Product P ($Da = 1$). The transport equation is normalized by d, U_J, and $\Gamma_{\alpha 0}$.

value in Fig. 29 because there is a large gradient in Γ_α in the interface normal direction. Thus, the interface normal component largely contributes to the change in Γ_α due to the relative velocity. The conditional profile of the interface normal component of this term is similar between A and P because both concentrations of A and P decrease toward the non-turbulent region in the interface normal direction. The large difference in this term can be seen between the trailing edge and the other two interfaces. The relative velocity $\mathbf{U}(\mathbf{x}^{\mathrm{I}} + \mathbf{x}_0^{\mathrm{I}}) - \mathbf{U}(\mathbf{x}_0^{\mathrm{I}}) - \mathbf{V}^{\mathrm{P}}$ in the non-turbulent region close to the interface is mainly determined by the $-\mathbf{V}^{\mathrm{P}}$ because the fluid velocity difference in this region is not as large as in the turbulent region. Therefore, the transport by the relative velocity is explained by considering the role of the interface propagation in the scalar transport in the local coordinate system as follows. The mean values of v_{n} at the cross-streamwise, leading, and trailing edges detected at $x/d = 15$ are $2.85 \times 10^{-3} U_{\mathrm{J}}$, $4.99 \times 10^{-3} U_{\mathrm{J}}$, and $-5.68 \times 10^{-3} U_{\mathrm{J}}$, respectively. Thus, only the trailing edge propagates toward the turbulent region on average. When the interface propagates toward the turbulent region, where Γ_{A} and Γ_{P} are large, Γ_{A} and Γ_{P} near the interface increases. Therefore, the transport due to the relative velocity is positive for A and P near the trailing edge especially in the non-turbulent region. In contrast, the propagation of the cross-streamwise and leading edges toward the non-turbulent region causes Γ_{A} and Γ_{P} near the interface to be decreased because of the small Γ_{A} and Γ_{P} in the non-turbulent region. The interface propagates toward the non-turbulent region when the enstrophy in the non-turbulent region near the interface increases. The non-turbulent region where Γ_{A} and Γ_{P} increase owing to the molecular diffusion and reaction becomes turbulent near the cross-streamwise and leading edges, and most of A and P are contained in the turbulent region. However, the inward motion of the trailing edge can leave the fluids containing A and P in the non-turbulent region. Because of this inward motion, there are fluids with a moderate scalar level in the non-turbulent region, which can be observed in the visualization in Figs. 11 and 13.

The difference between the trailing edge and the other two interfaces can be also seen in the adjustment layer, and this can be explained from the fluid velocity difference $\mathbf{U}(\mathbf{x}^{\mathrm{I}} + \mathbf{x}_0^{\mathrm{I}}) - \mathbf{U}(\mathbf{x}_0^{\mathrm{I}})$ because $\mathbf{U}(\mathbf{x}^{\mathrm{I}} + \mathbf{x}_0^{\mathrm{I}}) - \mathbf{U}(\mathbf{x}_0^{\mathrm{I}})$ largely contributes to the relative velocity in the turbulent region.[24] In the turbulent region, the transport by the relative velocity contributes to the increase in Γ_{A} and Γ_{P} near the cross-streamwise and leading edges but to the decrease near the trailing edge. Figure 31 shows the PDF of the relative velocity normal to the interface, $(\mathbf{U} - \mathbf{U}^{\mathrm{I}}) \cdot \mathbf{n}$, at $y_{\mathrm{I}} = -0.6$. The relative velocity is defined to be positive in the y_{I} direction. The relative velocity normal to the interface tends to be positive at $y_{\mathrm{I}} = -0.6$ near the cross-streamwise and leading edges, and the relative velocity in the turbulent region is frequently toward these interfaces. In contrast, the PDF of $(\mathbf{U} - \mathbf{U}^{\mathrm{I}}) \cdot \mathbf{n}$ shows a preference for a negative value near the trailing edge, and the relative velocity near the trailing edge is toward the turbulent core region. Because Γ_{A} and Γ_{P} are large in turbulent region, the relative velocity toward the interface contributes to the increase in Γ_{A} and Γ_{P} near the cross-streamwise and leading edges by transporting A and P in the turbulent core region toward the interface. In contrast, Γ_{A} and Γ_{P} in the adjustment layer near the trailing edge are decreased by the transport due to the relative velocity because the negative $(\mathbf{U} - \mathbf{U}^{\mathrm{I}}) \cdot \mathbf{n}$ transports the fluids

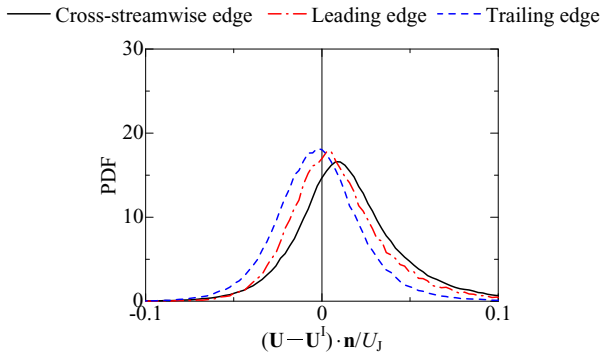

FIG. 31. PDF of relative velocity normal to T/NT interface in turbulent region ($y_{\mathrm{I}}/\lambda = -0.6$). The PDF is calculated for the interface detected at $x/d = 15$.

with small Γ_A and Γ_P near the trailing edge toward the turbulent region. It should be noted that the chemical reaction rate also depends on the interface orientation in the region where the difference in the transport due to the relative velocity appears. The large reaction rate near the cross-streamwise and leading edges is related to the relative velocity, which transports the deficient reactant A toward these interfaces. The larger concentration of P near the cross-streamwise and leading edges than near the trailing edge is also explained by the transport by the relative velocity, which contributes to the increase in Γ_P near these two interfaces. The large reaction rate near these two interfaces also causes the large Γ_P.

The difference in the relative velocity between the cross-streamwise and leading edges and the trailing edge is explained by considering the relationship between the interface geometry and the mean flow field. The leading (trailing) edge is located in the downstream (upstream) of the turbulent region. The turbulent fluid is characterized by the faster streamwise velocity than the non-turbulent fluid. Therefore, the relative velocity in the turbulent region is frequently toward the leading edge whereas the opposite tendency appears near the trailing edge. The non-turbulent fluids near the jet are dominated by the large-scale motions consisting of the induced flow and engulfing motion,[21] and move toward the jet flow. In contrast, the jet flow expands toward the non-turbulent region. Thus, the mean motion in the y direction is opposite between the turbulent and non-turbulent regions. These opposite motions make the relative velocity in the turbulent region toward the cross-streamwise edge. The mean flow field makes the relative velocity different among the three interface orientations. The chemical reaction near the interface is affected by the transport of the deficient reactant, which strongly depends on the relationship between the interface geometry and the mean flow field. Although the chemical reaction is isothermal in the present DNS, the dependence of reactions on the interface orientation is supposed to appear for reactions with heat release because this dependence is caused by the mean flow field, which is determined by the large scale motions.

IV. CONCLUDING REMARKS

The reactive scalar field near the T/NT interface was analyzed using a DNS of a planar jet with an isothermal second-order chemical reaction A + B → P. Reactants A and B are supplied from the jet and ambient flows, respectively. The DNS of the reactive jet was performed for three Damköhler numbers, $Da = 0.1$, 1, and 10.

A visualization of the T/NT interface and mixture fraction ξ shows that the T/NT interface successfully divides the flow field into regions of $\xi \approx 0$ and $\xi > 0$, and a large scalar dissipation rate of the mixture fraction appears along the T/NT interface. The T/NT interface also envelops the region where the product P exists, and most of P is contained in the turbulent region. The mean product concentration in the turbulent region for $Da = 1$ and 10 is large away from the jet centerline in the upstream region, and the product P exists in the entire turbulent region. The mean production rate in the turbulent region shows that the fast reaction occurs mainly away from the jet centerline, whereas the slow reaction occurs in the entire turbulent region.

The conditional mean concentration of the reactive species changes sharply near the T/NT interface. The width of the jump in the conditional mean concentration is similar to that in the conditional mean vorticity magnitude and is almost independent of the chemical species and Damköhler number. Near the T/NT interface, the reactant A, which is supplied from the jet flow, is deficient. Therefore, near the T/NT interface in the downstream region, most reactant A for $Da = 1$ and 10 has reacted, and only the reactant B and product P are contained in the fluid.

For the slow reaction ($Da = 0.1$), the conditional average of the chemical production rate gradually increases from the non-turbulent region toward the turbulent region. In contrast, it has a large peak value slightly inside the T/NT interface for $Da = 1$ and 10. This large peak in the production rate appears in the region where the conditional mean scalar dissipation rate of mixture fraction is large. The mixing of the two reactants near the trailing edge is close to the ideal state compared with that near the cross-streamwise and leading edges. However, the production rate is larger near the cross-streamwise and leading edges because the deficient reactant A is transported toward these two interfaces by the velocity relative to the interface movement. The relative velocity

also contributes to the increase in the concentration of P near the cross-streamwise and leading edges. The transport due to the relative velocity strongly depends on the relationship between the interface geometry and the mean flow field. Because of the dependence of the production rate and transport due to the relative velocity on the interface orientation, the concentration of P is large near the cross-streamwise and leading edges. The difference in the production rate among the three interface orientations becomes large as the Damköhler number increases. These results show that the characteristics of the T/NT interface greatly affect the fast reaction.

The cross-streamwise and leading edges propagate toward the non-turbulent region on average. When the interface propagates toward the non-turbulent region, the reactant A and product P remain contained in the turbulent region although the molecular diffusion and reaction contribute to the increase in the concentrations of A (non-reactive case) and P in the non-turbulent region. In contrast, the fluids containing A and P are left in the non-turbulent region by the interface propagation toward the turbulent region, which is often observed at the trailing edge.

ACKNOWLEDGMENTS

The authors acknowledge Professor C. B. da Silva and Mr. R. R. Taveira for providing valuable comments. The authors also acknowledge the anonymous referees for valuable comments. The authors would like to thank Dr. O. Terashima for his help in this study. Part of this work was conducted under the Collaborative Research Project of the Institute of Fluid Science, Tohoku University. This work was supported by JSPS KAKENHI Grant No. 25002531 and MEXT KAKENHI Grant Nos. 25289030, 25289031, and 25630052.

[1] J. C. Hill, "Homogeneous turbulent mixing with chemical reaction," Annu. Rev. Fluid Mech. **8**, 135 (1976).
[2] P. E. Dimotakis, "The mixing transition in turbulent flows," J. Fluid Mech. **409**, 69 (2000).
[3] R. W. Bilger, "Turbulent diffusion flames," Annu. Rev. Fluid Mech. **21**, 101 (1989).
[4] V. Zhdanov and A. Chorny, "Development of macro- and micromixing in confined flows of reactive fluids," Int. J. Heat Mass Transfer **54**, 3245 (2011).
[5] R. W. Bilger, "Future progress in turbulent combustion research," Prog. Energy Combust. Sci. **26**, 367 (2000).
[6] N. Peters, "Laminar flamelet concepts in turbulent combustion," Symp. (Int.) Combust., [Proc.] **21**, 1231 (1988).
[7] M. Gampert, V. Narayanaswamy, P. Schaefer, and N. Peters, "Conditional statistics of the turbulent/non-turbulent interface in a jet flow," J. Fluid Mech. **731**, 615 (2013).
[8] D. K. Bisset, J. C. R. Hunt, and M. M. Rogers, "The turbulent/non-turbulent interface bounding a far wake," J. Fluid Mech. **451**, 383 (2002).
[9] C. B. da Silva and J. C. F. Pereira, "The effect of subgrid-scale models on the vortices computed from large-eddy simulations," Phys. Fluids **16**, 4506 (2004).
[10] C. B. da Silva and J. C. F. Pereira, "Invariants of the velocity-gradient, rate-of-strain, and rate-of-rotation tensors across the turbulent/nonturbulent interface in jets," Phys. Fluids **20**, 055101 (2008).
[11] C. B. da Silva and R. R. Taveira, "The thickness of the turbulent/nonturbulent interface is equal to the radius of the large vorticity structures near the edge of the shear layer," Phys. Fluids **22**, 121702 (2010).
[12] C. B. da Silva, R. J. N. Dos Reis, and J. C. F. Pereira, "The intense vorticity structures near the turbulent/non-turbulent interface in a jet," J. Fluid Mech. **685**, 165 (2011).
[13] R. R. Taveira and C. B. da Silva, "Kinetic energy budgets near the turbulent/nonturbulent interface in jets," Phys. Fluids **25**, 015114 (2013).
[14] R. R. Taveira and C. B. da Silva, "Characteristics of the viscous superlayer in shear free turbulence and in planar turbulent jets," Phys. Fluids **26**, 021702 (2014).
[15] J. Westerweel, T. Hofmann, C. Fukushima, and J. C. R. Hunt, "The turbulent/non-turbulent interface at the outer boundary of a self-similar turbulent jet," Exp. Fluids **33**, 873 (2002).
[16] J. Westerweel, C. Fukushima, J. M. Pedersen, and J. C. R. Hunt, "Mechanics of the turbulent-nonturbulent interface of a jet," Phys. Rev. Lett. **95**, 174501 (2005).
[17] J. Westerweel, C. Fukushima, J. M. Pedersen, and J. C. R. Hunt, "Momentum and scalar transport at the turbulent/non-turbulent interface of a jet," J. Fluid Mech. **631**, 199 (2009).
[18] M. Holzner, A. Liberzon, N. Nikitin, B. Lüthi, W. Kinzelbach, and A. Tsinober, "A Lagrangian investigation of the small-scale features of turbulent entrainment through particle tracking and direct numerical simulation," J. Fluid Mech. **598**, 465 (2008).
[19] M. Holzner, B. Lüthi, A. Tsinober, and W. Kinzelbach, "Acceleration, pressure and related quantities in the proximity of the turbulent/non-turbulent interface," J. Fluid Mech. **639**, 153 (2009).
[20] M. Holzner and B. Lüthi, "Laminar superlayer at the turbulence boundary," Phys. Rev. Lett. **106**, 134503 (2011).
[21] J. Philip and I. Marusic, "Large-scale eddies and their role in entrainment in turbulent jets and wakes," Phys. Fluids **24**, 055108 (2012).
[22] T. Watanabe, Y. Sakai, K. Nagata, O. Terashima, H. Suzuki, T. Hayase, and Y. Ito, "Visualization of turbulent reactive jet by using direct numerical simulation," Int. J. Model. Simul. Sci. Comput. **04**, 1341001 (2013).

[23] T. Watanabe, Y. Sakai, K. Nagata, Y. Ito, and T. Hayase,"Wavelet analysis of coherent vorticity near the turbulent/non-turbulent interface in a turbulent planar jet," Phys. Fluids **26**, 095105 (2014).
[24] T. Watanabe, Y. Sakai, K. Nagata, Y. Ito, and T. Hayase, "Vortex stretching and compression near the turbulent/non-turbulent interface in a planar jet," J. Fluid Mech. **758**, 754 (2014).
[25] T. Watanabe, Y. Sakai, K. Nagata, Y. Ito, and T. Hayase, "Enstrophy and passive scalar transport near the turbulent/non-turbulent interface in a turbulent planar jet flow," Phys. Fluids **26**, 105103 (2014).
[26] Y. Morinishi, T. S. Lund, O. V. Vasilyev, and P. Moin, "Fully conservative higher order finite difference schemes for incompressible flow," J. Comput. Phys. **143**, 90 (1998).
[27] P. R. Spalart, R. D. Moser, and M. M. Rogers, "Spectral methods for the Navier-Stokes equations with one infinite and two periodic directions," J. Comput. Phys. **96**, 297 (1991).
[28] T. Watanabe, Y. Sakai, K. Nagata, O. Terashima, and T. Kubo, "Simultaneous measurements of reactive scalar and velocity in a planar liquid jet with a second-order chemical reaction," Exp. Fluids **53**, 1369 (2012).
[29] T. Watanabe, Y. Sakai, K. Nagata, and O. Terashima, "Joint statistics between velocity and reactive scalar in a turbulent liquid jet with a chemical reaction," Phys. Scr. **T155**, 014039 (2013).
[30] T. Watanabe, Y. Sakai, K. Nagata, and O. Terashima, "Turbulent Schmidt number and eddy diffusivity change with a chemical reaction," J. Fluid Mech. **754**, 98 (2014).
[31] T. Watanabe, Y. Sakai, K. Nagata, and O. Terashima, "Experimental study on the reaction rate of a second-order chemical reaction in a planar liquid jet," AIChE J. **60**, 3969 (2014).
[32] M. van Reeuwijk and M. Holzner, "The turbulence boundary of a temporal jet," J. Fluid Mech. **739**, 254 (2014).
[33] Y. Dai, T. Kobayashi, and N. Taniguchi, "Large eddy simulation of plane turbulent jet flow using a new outflow velocity boundary condition," JSME Int. J., Ser. B **37**, 242 (1994).
[34] S. B. Pope, *Turbulent Flows* (Cambridge University Press, Cambridge, 2000).
[35] M. Klein, A. Sadiki, and J. Janicka, "A digital filter based generation of inflow data for spatially developing direct numerical or large eddy simulations," J. Comput. Phys. **186**, 652 (2003).
[36] M. Gampert, K. Kleinheinz, N. Peters, and H. Pitsch, "Experimental and numerical study of the scalar turbulent/non-turbulent interface layer in a jet flow," Flow, Turbul. Combust. **92**(1-2), 429–449 (2014).
[37] R. W. Bilger, "Some aspects of scalar dissipation," Flow, Turbul. Combust. **72**, 93 (2004).
[38] H. Tsunoda, Y. Sakai, I. Nakamura, and S. Liu, "The effect of a circular cylinder on the diffusion of matter by a plume," J. Fluid Mech. **246**, 419 (1993).
[39] R. R. Taveira, C. B. da Silva, and J. C. F. Pereira, "The dynamics of turbulent scalar mixing near the edge of a shear layer," J. Phys. Conf. Ser. **318**, 052049 (2011).
[40] R. W. Bilger, L. R. Saetran, and L. V. Krishnamoorthy, "Reaction in a scalar mixing layer," J. Fluid Mech. **233**, 211 (1991).
[41] S. Komori, T. Kanzaki, and Y. Murakami, "Concentration correlation in a turbulent mixing layer with chemical reactions," J. Chem. Eng. Jpn. **27**, 742 (1994).
[42] A. D. Chorny and V. Zhdanov, "Turbulent mixing and fast chemical reaction in the confined jet flow at large Schmidt number," Chem. Eng. Sci. **68**, 541 (2012).
[43] R. R. Taveira, J. S. Diogo, D. C. Lopes, and C. B. da Silva, "Lagrangian statistics across the turbulent-nonturbulent interface in a turbulent plane jet," Phys. Rev. E **88**, 043001 (2013).